Microwave electromagnetic modelling of Sahelian-grassland

A. Monsivais-Huertero, I. Chênerie, K. Sarabandi, Frédéric Baup, Éric Mougin

Microwave electromagnetic modelling of Sahelian-grassland

A. MONSIVAIS-HUERTERO*†, I. CHENERIE†, K. SARABANDI‡, F. BAUP and E. MOUGIN

†Laboratoire d'Etudes et de Recherche en Imagerie Spatiale et Médicale, UFR PCA, Université Paul Sabatier Toulouse III, 118 route de Narbonne, 31062 Toulouse CEDEX 9, France

‡Radiation Laboratory, Department of Electrical Engineering and Computer Science, The University of Michigan, Ann Arbor, Michigan 48109-2122, USA

*Corresponding author. Email: monsivais@ufl.edu

Abstract

In this paper radar scattering models based on coherent and incoherent formulations for an African grassland (Sahelian) are examined. The coherent model is used to account for the structure of the grass plants and the results are compared with the same model assuming random placement and orientation of scatters, and the Radiative Transfer model. The validity of the three models applied to grass vegetation is determined by comparing the model predictions with ENVISAT ASAR data gathered in 2005 over Sahelian grassland. The Agoufou site, as defined in AMMA project, is selected as the test target and a set of ground data were collected during 2004 and 2005.

Through a comprehensive data comparison, it is shown that the coherent scattering model with a generator considering botanical information is the best model to predict the backscattering data that matches ENVISAT measurements well (correlation = 0.92). At low incidence angles (<30°), the radar backscatter shows a strong dependence to soil moisture variations. The analysis of the different contributions leads to study the main scattering mechanisms. For high incidence angles, backscattering coefficient at HH polarization shows a marked seasonal variation associated to grass presence.

1. Introduction

In recent years, much research in radar remote sensing has been focused on forested environment because of its fundamental importance in carbon cycle and the Earth climate dynamics. However, another important class of vegetation cover is grassland (less than 5% tree cover over the total surface of the study site) that has not received the attention it deserves with regards to its role in

carbon cycle. Most of recent radar studies dealing with short vegetation pertain to cultural grassland (Touré et al. 1994, Picard et al. 2003, Taconet et al. 1994, Bouman 1991, Ferrazzoli 1992, Stiles and Sarabandi 2000, Stiles et al. 2000) and only a handful in open literature have focused on natural grassland (Frison et al. 1998, Jarlan et al. 2002, Frison et al. 2000, Saatchi et al. 1994, Bakhtiari and Zoughi 1991). Dry and sub-humid lands are found throughout the world with total coverage of approximately 47% of the world's terrestrial area of which 74% is covered by grassland and savannah (White and Nackoney 2002). As a significant portion of the Earth's dry and sub-humid land is covered with natural grassland, a global monitoring of the grassland ecosystem and it dynamics is highly desirable.

Different models have been proposed employing either analytical or semi-empirical modelling to predict and understand the grassland dynamic (Touré et al. 1994, Picard et al. 2003, Ferrazzoli 1992, Stiles and Sarabandi 2000, Stiles et al. 2000bis, Jarlan et al. 2002, Frison et al. 2000). The structure of grass vegetation leads to many interesting phenomena that make the application of random media scattering techniques problematic. When dealing with grass vegetation, the small structure of grass can produce an electrically small scattering volume at microwave frequencies. Furthermore because of element closeness, the total scattering power cannot be reduced to an addition of scattering power from each separate plant. The canonical elements used in the models depend on the available ancillary data and the complexity of the grass structure.

A majority of the world's savannah and grassland ecosystems are located in Africa encompassing approximately 14.5 million km^2. The study site, named Agoufou is located within the AMMA (African Monsoon Multidisciplinary Analysis) mesoscale site 14.5° - 17.5°N, 1° - 2°W in the Gourma region in Mali (AMMA 2002). Ground data for this site were collected during measurement campaigns in 2004 and 2005. In a previous work (Frison et al. 1998), Frison et al. have modelled the Sahelian grassland using a semi-empirical backscattering model based on the radiative transfer method. In this paper, the effect of backscattering from grass and shrubs were totally ignored assuming dry condition and low volume fraction. It is shown that green grass with sufficient moisture content at L-band and above can produce significant backscatter (Stiles and Sarabandi 2000, Stiles et al. 2000). In these same papers it is shown that the backscatter is a function of semi-deterministic grass structure which give rise to what is known as phase-coherent effects. The coherence of backscatter from different parts of the plant structure can have a significant effect on the overall scattering from grassland.

ENVISAT satellite was launched in 2002 by the European Space Agency (ESA), one of its on board instruments is Advanced Synthetic Aperture Radar (ASAR) operating at C-band capable of collecting data at different angles and polarizations. The satellite has a 35-day repeat pass cycle. The angular diversity allows for observing the same site at different incidence angles over a long period of time. This characteristic is a helpful feature that facilitates the accurate estimation of soil moisture content (Zribi and Dechambre 2003). However, to understand seasonal vegetation dynamics, this angular diversity imposes an additional task: the angular normalization of the gathered data. This is an important task as the output product (estimation of the biophysical parameters for the SAR data) is also dependent on the accuracy of the angular normalization algorithm.

The aim of this study is to improve the understanding of the Sahelian grassland dynamic by using a coherent model adapted to this class of vegetation. This paper presents a comparison between

three different formulations to predict the radar response from Sahelian vegetation: a coherent formulation considering botanical information of the grassland (Monsivais-Huertero et al. 2007), a coherent formulation representing the vegetation as a random medium (Thirion et al. 2004), and an incoherent approach (Ulaby et al. 1988). The paper is organized in 6 sections. Section 2 presents different electromagnetic mode1s used to construct the grassland model. The description of the test site is provided in Section 3. Section 4 describes the methodology employed to compare the coherent models with a Radiative Transfer model (MIMICS) and Section 5 presents the comparison of the three models predications against ENVISAT HH-polarized data. Soil moisture content dependence is presented in Section 6. And finally, conclusion remarks are provided in Section VII.

2. Electromagnetic modelling

2.1. Soil modelling

The most common analytical backscattering models used to study the radar response from natural surfaces are the Kirchoff approximations and the small perturbation model (Ulaby et al. 1986), however their range of validity is limited (Ogilvy 1991, Fung 1994). Fung et al. (Fung et al. 1992) developed the Integral Equation Model (IEM) which provides wider range validity than the aforementioned models. In later studies, comparisons of IEM simulations and data acquired during radar campaigns have shown the limits of this model (Zribi et al. 1997, Zribi et al. 2000, Rakotoarivony 1996). In recent years, different improvements to this model have been reported in (Zribi and Dechambre 2003, Chen et al. 2000, Hsieh et al. 1997). In (Zribi and Dechambre 2003), Zribi et al. proposed to add a new roughness parameter $Z_s = h_{rms}^{\ 2} / l_c$ in order to mix the effects of the rms height (h_{rms}) and the correlation length (l_c) and introduce the slope effect. The results show a small error in simulations of the radar response in a range from 0.0007 to 1.93 cm of Z_s (correlation = 0.9857).

In this study we deal with a dry surface and its response is obtained by an incoherent version of the IEM model with the improvements mentioned in (Zribi and Dechambre 2003).

2.2. Vegetation model

To analyse the vegetation contribution, we compare the backscattering coefficient from three different models: a coherent formulation with a specific generation for African vegetation (Monsivais-Huertero et al. 2007), a coherent formulation with a uniform-distribution generation (Thirion et al. 2004) and the MIMICS code (Ulaby et al. 1988) which is based on the Radiative Transfer Theory. These three models use a discrete representation of vegetation. They consider it as a cluster of different types of scatterers which model the vegetation elements (leaves,

branches, trunks, etc.). Each scatterer type is described by its dimensions, its spatial density, and its moisture content.

In these electromagnetic formulations, multiple scattering effects are ignored and the scattering mechanisms considered are the direct scattering and the vegetation-ground interaction. The coherent formulations (sections 2.2.1 and 2.2.2) calculate the vegetation-ground interaction as the contribution given by the ground-scatterer scattering, the scatterer-ground scattering, and the ground-scatterer-ground scattering (Figures 2 and 4), whereas MIMICS supposes the following mechanisms to calculate that interaction: ground-cover-ground scattering, cover-ground scattering, ground-cover scattering, trunk-ground scattering, and ground-trunk scattering (Figure 5). The vegetation-ground interaction is going to be called double scattering in this paper.

For all models, the inputs are the scatterer description, the number and height of layers, the rough-surface description and radar parameters. Dielectric constants for vegetation and soil are calculated by the formulas developed in (Ulaby and El-Rayes 1987) and (Peplinski et al. 1995), respectively. Four angle parameters are used to define the incidence angle and scattering angle: θ_s and ϕ_s are for scattering direction and θ_i and ϕ_i are for the incidence direction. The outputs are the backscattering coefficient, the contribution from different scatterers and contribution from different scattering mechanisms.

2.2.1. Coherent scattering formulation and specific generator for African vegetation.

This formulation is based on the model presented in (Monsivais-Huertero et al. 2007) in which authors propose a coherent formulation using a specific generator for the African savannah. In order to simulate realistic vegetation structure, detailed botanical description is incorporated into the vegetation generation. Sahelian grassland is mainly composed of annual herbaceous plants and woody shrubs. In this generator, only the two dominant species are taken into consideration: Cenchrus biflorus and Leptadenia pyrotechnica for shrubs (figure 1).

The species Cenchrous biflorus (grass) presents a particular structure which changes with time. In this growth process, three stages can be defined: seedling, adult plant, and dry plant. To generate grasses, a 3D structural model considering the changes during their growth process is implemented. The generator represents the grass as a set of cylindrical stalks and blade leaves (see Figure 1). The generation of shrubs is made considering stratified layers, each having a specific volume fraction and size distribution. The structure is reproduced from the bottom to the top. Elements enclosed in an upper layer are related to location of elements contained in the previous lower layer in order to reproduce a realistic description of the tree morphology. The physical parameters of the elements inside envelops are described by length, radius, orientation, and dielectric properties. The statistics of these parameters and the associated number densities are determined from the ground truth data (see Figure 1).

Once the grassland is created, it is treated as a cluster of scatterers composed of cylinders (trunks, branches, and stems) and blades (grass leaves). The scattered field from cylindrical elements is calculated using the infinite cylinder approximation (Ulaby and Elachi 1990) and for blade elements the polarizability tensor formulation is used (Stiles et al. 1993). The entire elements

(shrubs and grasses) are illuminated by plane wave, and the scattered field in the far zone is evaluated.

In the case of shrub structures, the scatterers are considered to be embedded in an elliptical envelop and/or in a cylindrical envelop depending on shrub shape, the extinction of the coherent wave is then calculated only when travelling in the volume contained within the envelops. For grass structure, multiple scattering among adjacent elements can be neglected at microwave frequencies. Also grass plants are independent of each others and thus their covariance matrix can be added. The backscattering coefficient is proportional to the average covariance matrix multiplied by the grass number density. For simulations, the mean field at a given point within the grass layer, which accounts for the attenuation and phase change due to the scattering and absorption losses of vegetation particles, is calculated using the Foldy's approximation (Tsang 1985). Finally the total backscattering from the Sahelian scene is computed by adding the contribution of shrubs, grass and soil (Figure 2).

2.2.2. Coherent scattering formulation and uniform-distribution generator.

This vegetation modelling is based on a coherent model for forest scattering (Thirion et al. 2004), which has been adapted for grassland. In this model, the vegetation is described as a discrete medium placed on a dielectric soil with rough interface. The vegetation medium is modelled by a multi-layer random media each defined according to their particle shape distribution and number density as shown in Figure 3. The vegetation is represented as a cluster of scatterers composed of smooth dielectric cylinders of circular cross section to simulate branches and stalks and thin dielectric ellipsoids to reproduce leaves (Ulaby and Elachi 1990, Karam and Fung 1989). To preserve the geometrical feature of grass plants a vegetation generation model is constructed that provides the description scatterers within each layer. The generator uses also the spatial description (orientation and position) to create the vegetation. The model was adapted by removing the generation of the first layer containing trunks and the location of scatterers inside a volume representing the tree crown. Instead, the adapted model places the scatterers following a uniform distribution. The scatterers' orientation is determined according to the ground data. The phase center of scatterer is located within the grass layer determined in terms of the grass height using a uniform distribution. Additionally, we consider that grass leaves are random enough to neglect the effect of their relative positions on scattering. As far as shrubs are concerned, they are generated as a forest canopy.The scatterers are positioned taking into consideration the no-superposition condition among elements enforcing a minimal distance between them and using a probabilistic function to have a realistic distribution.

The mean field in each layer is used as the illuminating field for the scatteres using Foldy's approximation (Tsang 1985) which accounts for the attenuation as well as phase shift of the incident and reflected fields as they go through the layered effective media representation the vegetation layers. Soil backscatter contribution is modified by taking into account the attenuation due to vegetation layers above it. A flow chart of the model is shown in Figure 4.

Finally, the total backscattering coefficient (σ^0) is the addition of the vegetation contribution and the soil contribution. An average backscattering-coefficient value is obtained by performing

the backscattering coefficient over several realizations to warrant the convergence of the response.

2.2.3. Michigan Microwave Canopy Scattering (MIMICS).

The MIMICS backscattering model uses radiative transfer theory to describe the backscattering behaviour of a forest. This theory is suitable for a medium like vegetation where scatterers have discrete configurations and dielectric constants much larger than that of the air (Ulaby et al. 1988). Geometrically, the tree canopy is divided into three regions: the crown region, the trunk region, and a rough-surface ground boundary (Figure 5). The crown region is composed of several types of scatterers. This inhomogeneity is accounted for by averaging the Stokes matrix over the statistical distributions which characterise the sizes, shapes, and orientations of the canopy elements.

We adapted MIMICS model to the African vegetation by eliminating the contributions from trunks (Touré et al. 1994) when computing the grass backscattered signal. In addition, grass stems and grass leaves are represented as contained in the same region (cover layer). The shrubs are generated as a tree canopy. The overall backscattering from the Sahelian vegetation is computed by adding the contribution of shrubs, grass and soil. For simulations, we use botanical parameters presented in section 3.1, and the soil contribution is calculated by a simplified version of the IEM method presented in (Zribi and Dechambre 2003). As far as scattering formulation of grass elements is concerned, MIMICS models uses the Rayleigh Gans approximation to calculate the scattering matrix from elliptical geometries (Ulaby et al. 1990).

Although MIMICS had not been tested for this type of vegetation before, it has been validated using a large variety of cases showing great results (Ulaby et al. 1988, McDonald et al. 1990, McDonald and Ulaby 1993, Beauchemin 1995, Liang 2005, Liang 2005bis).

3. Data collection

3.1. Ground data

The study site is located in Northern Mali, in the Gourma region. Its geographical coordinates are 15.35°N and 1.48°W.

The Agoufou site is steered by a semi-arid tropical climate defined by the water resources, the day duration and the temperature amplitude. The rainy season, during the African monsoon, generally starts at the end of June and finishes in September. The vegetation dynamic is mainly determined by rainfall during the monsoon (Tracol 2004). Vegetation development starts after the first rain (not prior to June) and unless the annual plants wilted before maturity due to lack of

rain, the senescence follows the fructification that matches with the end of the rainy season. This vegetation is composed of shrubs (1% cover), trees (3% cover) and annual herbaceous layer (5-40% cover). Exposed soil range is between 60 % and 95% depending on the season. During the dry season (from October to June), there is no green vegetation apart from exception of shrubs and trees. Trees can be classified into four species: Acacia Senegal (0.15% cover), Acacia raddiana (0.35% cover), Balanites aegyptica (0.25% cover), Combretum (0.15% cover) and Leptadenia pyrotechnica (2.99% cover) which is the main species. The grass species are Cenchrus biflorus and Zornia gloochidiata. In this study only Leptadenia pyrotechnica and Cenchrus biflorus are considered (see figure 6).

In (Mougin et al. 1995), a botanical description of Sahelian vegetation is given in terms of herbaceous biomass, environmental parameters, water budget, etc. In this study, we are only focused on grass density, grass geometrical properties and grass dielectric properties such as moisture content. In the particular case of density calculation, we use equations (26) – (28) given in (Mougin et al. 1995) that link the grass biomass and LAI to grass density. Ancillary data were gathered during two experimental campaigns in 2004 and 2005 along a 1ha area as a part of the AMMA project (AMMA 2002, Baup 2007). We assume that branch and trunk moistures are constant throughout the year and are set at 50% and 60%, respectively. Their geometrical characteristics are shown in Table I (Jarlan et al. 2002, Baup 2007). The herb description is shown in Table II (Jarlan et al. 2002, Baup 2007) and Table III (Mougin et al. 1995, Baup 2007). During the 2005 experimental campaign, parameters have been measured (biomass, geometrical dimensions of shrubs, soil moisture content). Then, these values were used to calibrate a vegetation growth model (Mougin et al. 1995). Once the growth model was calibrated, it was used to obtain the input parameters for the radar coherent model. As well, we show volumetric soil moisture content and green herb height in Table III.Geometrical grass parameters were taken from (Jarlan et al. 2002). Additional parameters for the coherent model using a specific generator are given in Table IV.

For the model with uniform generator and MIMICS, angles α, β, and γ represent the Eulerian angles of the orientation of disc axis. The angle β follows an erectophile distribution ranging between 0° - 35° (Table III). These values are taken from (Jarlan et al. 2002). For the model with a specific generator, since it considers the relative position between elements, the Eulerian angles are fixed and their values are obtained from statistics of samples taken during the experimental campaign (Table IV). The categories of stalks and stems presented in Table IV correspond to the grass structure shown in Figure 1.d. Each category corresponds to one segment in which the grass element (stem or leaf) is discretized.

In (Jarlan et al. 2002), it is shown that stalk contribution is significantly lower than grass contribution at C-band and thus, it could be neglected. Based on this result and due to the lack of stalk measured data, we also neglect stalk contribution when representing the vegetation as a uniform-distributed medium.

Soil moisture content values are estimated using the STEP model (Mougin et al. 1995). Due to the components of the measured soil in the test site, the measured moisture content values present a significant dynamic range (figure 6e).

The soil is essentially composed of sand (91.2%) and of clay (4.5%) (Tracol 2004). During the 2005 campaign, roughness measurements were made using a pin profiler (with a total length of 2m and a resolution of 1 cm). About 20 profiles of bared soil were taken in order to guarantee enough accuracy in the surface roughness estimation. For each profile we computed the correlation function (Ogilvy 1991) and derived the two statistical parameters, obtaining the rms height (h_{rms}) as $8.5\ mm$ and the correlation length (l_c) equal to $274.0\ mm$. As well, it was found that the correlation function describing the soil surface is exponential.

In this study, the characteristics of both trees and soil roughness are assumed to be constant throughout the year.

3.2. ENVISAT-ASAR data

ENVISAT satellite was launched in March 2002 by ESA (European Space Agency). It is on a sun-synchronous orbit at a mean altitude of 800 km. The satellite has a repeat cycle of 35 days. ENVISAT ASAR radar is a multi-mode sensor operating at C-band (5.3 GHz), capable of providing all polarization configurations (VV, VH, HV and HH), incidence angles and spatial resolution. The ASAR instrument can operate as a strip-map SAR (Image and Wave Modes) or as a ScanSAR (Global Monitoring, Wide Swath and Alternating Polarization modes) (ESA 2004).

ENVISAT ASAR images of the site Agoufou were acquired in Wide Swath mode (WS) for several dates of 2005 with incidence angles between 15° and 45° at VV polarization from 16 January to 5 June and at HH polarization from 16 July to 26 October (table V). Absolute calibration of these images is carried out to transform the radar signal into a backscattering coefficient using B.E.S.T. (Basic ENVISAT SAT Toolbox) program (BEST 2005). The confidence interval is $\pm$ 0.6 dB.

4. Numerical comparison of models

4.1. Methodology

Since the Agoufou site is composed of shrubs and grass, the scattering model is run for two types of vegetation cover. The vegetation generator tool contained in each model generates tree structure to model the shrubs and grass structures for different growing stages. As there are no significant electromagnetic interactions among sparse shrubs and the grass plants the backscattering coefficient of the Sahelian grassland is obtained by adding the backscattering coefficients from the trees and the grass incoherently in all models.

As ellipsoid scattering (leaves) is calculated by means of the generalized Rayleigh Gans approximation, it should be verified that at least, one dimension of leaf scatterers is much smaller than the wavelength or kc<<1 where c is the smallest dimension and k is the wave number. Since we are working at C-band, the factor kc is 0.033 that is much smaller than 1, then the condition of the generalized Rayleigh Gans approximation is validated.

For the coherent formulations, the backscattering coefficient is obtained by averaging the backscatter radar cross section from adequate number of statistically independent trees divided by the tree number density. In these Monte Carlo simulations, it is necessary to perform a convergence test for each type of vegetation (shrubs and grass) to ensure data accuracy. For shrubs structure, a convergence value is reached for 50 realizations for both two coherent formulations whereas for grass, it is necessary, to include at least 100 realizations for the uniform generator and 400 when we use the specific generator.

In order to observe the influence of a coherent formulation and a specific generation taking into account botanical information, we present two comparative studies: 1) comparison between a coherent formulation with a specific generator (section 2.2.1) and a coherent formulation with a uniform-distribution generator (section 2.2.2), and 2) comparison between a coherent formulation (section 2.2.1) and the MIMICS model (section 2.2.3). When comparing the backscattering coefficient predicted by the coherent model and that by MIMICS, we need to have in mind that these models employ two different generators. So, the differences observed should be interpreted in a qualitative way instead of a quantitative one. All the models are evaluated at 2 incidence angles: 23° (low incidence) and 40° (high incidence).

Since the models consider different generations and canonical representations of scatterers, these differences contribute to produce diverse outputs, thus it is difficult to single out the effects of coherent interactions from several other effects. In this analysis, we study comparatively the differences between the backscattering coefficients from the contributors (grass, shrubs, and soil) obtained by the three models.

In addition, to validate the different models, a comparison between their results and the measured ENVISAT-ASAR data is presented. Due to the homogeneity of the land surface, backscattering coefficient is estimated over a 1 x 1 km² area, by averaging over 180 pixels, which implies a radiometric error of $\pm$ 0.6 dB (Baup et al. 2007).

4.2. Surface scattering model

Figure 7 shows the comparison between the IEM model and the ENVISAT ASAR data at VV polarization during the dry season (no green vegetation). For this simulation, the mean soil moisture content during the dry season is considered equal to 0.7% (εr = 3.62). The correlation between simulations and measured data is r = 0.67 for VV polarization and r = 0.9414 for HH polarization. According to theses results, IEM best agrees with the measure data at the lower incidence angles and for VV polarization. As the incidence angle increases, the error between measurements and IEM increases. The mean error for low incidence angles (10° - 30°) is 1 dB

whereas for high incidence angles it reaches up to 4 dB for both polarizations. This error is attributed to the variability in surface roughness parameters over a large area from which the backscatter data was collected (1km X 1km). The backscatter coefficient is not very sensitive to correlation length.

This is only a partial validation because it is necessary to compare with a larger number of measured points for both two polarizations. In order to carry out this study, we consider that this accuracy is enough to try to understand the Sahelian grassland dynamic.

4.3. Comparison between a specific generator and a uniform generator for a coherent formulation

To evaluate the effects due to a specific generation to represent the African vegetation, we compare the contributions obtained by two coherent models. The first one considers a generator based on botanical information (Monsivais-Huertero et al. 2007) and the second one supposes a uniform spatial distribution of vegetation elements (Thirion et al. 2004). The results for incidences at 23° and 40° are shown in figures 8 and 9, respectively.

4.3.1. 23° incidence angle. Observing the scattering contributions at 23° for both two models, the major component is the backscattering from soil for HH and VV polarizations. Thus, the total backscattering coefficient describes mainly the behaviour of the soil surface as a function of soil moisture content. Total contribution depicts similar behaviour and levels for all polarisations according to the two models. The main contribution for each case is summarised in Table VI. The significant variation of this ground parameter does not allow careful examination of seasonal variation attributed solely to vegetation contribution. Even though, this seasonal dynamic is well depicted by grass contribution which describes the growth-grass period.

For shrubs, both models predict similar level and same behaviour. The double scattering is higher than the direct scattering. Both models show a similar difference between these two mechanisms.

For grass, the models show opposite behaviour. Whereas the model with a specific generator predicts a higher contribution of the double scattering than that of the direct scattering, the model with a uniform generator obtains that the dominant mechanism is the direct scattering. This could be explained by the scatterers' orientation, since the direct scattering occurs only when the wave incidences perpendicularly on the scatterer, this phenomenon happens more times when considering a random distribution.

4.3.2. 40° incidence angle. In order to observe the influence of grass structure on the total backscattering coefficient, a study at 40° incidence angle is carried out. At this incidence, as it was reported by other authors (Zribi and Dechambre 2003, Ulaby et al. 1980), the radar signal shows marked seasonal variation associated with the development and senescence of annual grass during the rainy season. The different stages of grass growth are well depicted by the curve in the two models. Comparing the two models, it is observed that the grass contribution has a higher contribution when considering a more realistic generator.

As it is expected, the HH-polarized radar signal at 40° shows a more marked seasonal variation associated with the development and senescence of annual grass during the rainy season. The different stages of grass growth are depicted by the curve from both models, even though the dynamic shown by the model with a specific generator is slightly higher (Table VII). This increment in the dynamic is because the double scattering is higher than the soil contribution when representing the vegetation with a specific generator, so the grass seasonal variation is more visible.

For VV polarization, both models predict that the major contribution comes form the soil, thus, the radar signal does not show a significant seasonal dynamic indicating the presence of grass.

For shrubs, also at this incidence both models show similar levels and same behaviour. For grass, as at 23° incidence, the double scattering is higher than the direct scattering according to the model with a specific generator, whereas the model with a uniform distribution predicts opposite behaviour.

The difference between the grass direct scattering obtained by the uniform generator and that by the code with the specific generator is about 20 dB at VV polarization, 25 dB at HH polarization, and 7 dB at HV polarization for both incidence angles. For the grass double scattering, both models predict similar levels at 23°, but at 40°, the value from the model with a specific generator is higher. This difference as a function of the incidence angle is because the contribution of the double scattering increases as the incidence angle also increases, so botanical information of plant structure has a more significant role in the scattering calculation.

In conclusion, the use of botanical information to represent the vegetation influences the nature of the main contribution of grass.

4.4. Comparison between a coherent formulation and an incoherent formulation

In order to observe the effects due to a coherent formulation and a specific generator, we compare the results by the coherent model developed in (Monsivais-Huertero et al. 2007) and those by MIMICS (Ulaby et al. 1988). The dominant contributors are summarised in Table VIII for each studied configuration. Figures 10 and 11 present the radar response obtained by the coherent model with a specific generator and by MIMICS at 23° and 40° incidence angles, respectively.

4.4.1. 23° incidence angle. At 23° incidence, the major contribution comes from the soil for both two formulations (coherent and incoherent) at two co-polarizations (Table VIII). As the two formulations employ the same surface scattering model, the seasonal variation of the backscattering coefficient from the two models is the same. At HV polarization, the major contribution comes from grass according to results by the coherent formulation and from shrubs according to MIMICS.

For shrubs, the two formulations obtain inverse behaviour for the scattering mechanisms. MIMICS model gets a higher level for the direct scattering whereas the coherent model predicts a higher level for the double scattering (Figure 10). The difference between the two scattering

mechanisms is more significant in the coherent formulation. Despite this difference in the formulations, it does not modify the seasonal variation of the overall backscattered signal at co-polarization because of the low amplitude of shrub contribution (about -30 dB). The opposite behaviour in the scattering mechanisms can be explained by the presence of coherent effects in the shrub structure. As mentioned in (Saatchi and McDonald 1997), when comparing a coherent formulation and a incoherent formulation, the factor called "coherent", which is related to the calculation of double scattering, takes into account constructive interference of the travelling wave, increasing in this manner the contribution of this mechanism.

For grass, also inverse behaviour is observed. Moreover, the total contribution from grass obtained by the coherent formulation has a higher level than that get by MIMICS. This increment in the amplitude of the grass contribution is due to an increment in the double scattering.

Table IX shows the dynamic obtained by each formulation. It is observed that in cases in which the main contribution is the soil, both two formulations produce similar dynamic. This is because at this incidence, seasonal variations of grass are not visible in the shape of the total backscattering coefficient.

4.4.2. 40° incidence angle. At this incidence angle, the major contribution for MIMICS continues being the direct scattering from soil (Table VIII). In any case, MIMICS predicts a seasonal variation due to the grass presence as the coherent model does at HH polarization for this incidence.

At HH polarization, the difference between the calculation of the double scattering from grass by the two formulations increases in comparison with 23° incidence angle. Observing Figures 10 and 11, both two models obtain similar levels at co-polarization for direct scattering from grass. The difference in the calculation of double scattering could be attributed to coherent effects due to grass structure that are neglected in MIMICS (Stiles et al. 2000).

Observing curves of figures 8 - 11, the only one where grass signature has a significant effect is at 40° incidence angle and HH polarization. Thus, this is a curve that might be used for an eventual implementation of a retrieval algorithm for grass parameters. The other curves could be useful to retrieve soil parameters.

For all cases and at VV polarization, unlike canopy vegetation where vegetation scattering is higher than soil scattering, simulations of African vegetation show that the main contribution comes from soil. This opposite behaviour could be attributed to different reasons. The first one is the scatterers' geometry and scatterers' orientation. In the case of canopies, they are composed of branches and trunks with cylindrical geometries and well defined orientation, and elliptical leaves with small dimensions and random orientation; in contrast, grassland is mainly composed of blade leaves with bigger dimensions and an orientation range more restricted. Another reason is the vegetation height, canopies have a height of meters, and on the contrary grass height is about 40 cm. A third reason is the low vegetation cover in Africa savannah that is related to direct scattering.

From these results, it is possible to conclude the existence of compensation effects. Although the levels of the backscattering coefficient are similar by the three models, they predict different main contributions. For instance, at HH polarization and 40° incidence, the coherent formulations obtain as the main contribution the grass and MIMICS obtains the direct scattering from soil. When taking into account a coherent formulation and botanical information in the vegetation generator, it is get an increment in the contribution of double scattering from grass. However, in our case, the presence of vegetation is low, so at low incidence these enhancements in vegetation modelling do not produce a significant difference in comparison to the radar response predicted by other models. In contrast, at high incidence, the modelling proposed in (Monsivais-Huertero et al. 2007) evidences a higher contribution of double scattering from grass.

5. Comparison of the different models with ENVISAT data

Figure 12 shows the comparison of the coherent code with a specific generator, the coherent model with a uniform-distribution generator, MIMICS, and ENVISAT-ASAR data. As ENVISAT satellite has a 35-day repeat cycle, measurements of consecutive days are collected at different incidence angle. Thus, each day is simulated using vegetation and soil parameters shown in Tables I – IV for a particular incidence angle in order to match with that recorded by the satellite.

When considering the angles reported in Table V, the correlation achieved by the coherent model using a specific generator is r = 0.92, the coherent model with a uniform distribution gets a correlation r = 0.896, and the correlation using MIMICS is only r = 0.64.This can mainly be attributed to the plant structural dependent coherence effects which are neglected in the Radiative Transfer model and when using a random generator (Stiles et al. 2000, Frison et al. 1998, Saatchi and McDonald 1997). It is observed that the model based on a coherent formulation and taking into account botanical information in the vegetation generator is the model that best matches with ENVISAT data, with a correlation coefficient of 0.92. The maximum difference between the measured data and the coherent model with a specific generator is 3.7 dB for September 18th (day 261, θi = 42.08°), the coherent model with a uniform generation is about 3.6 dB for September 8th (day 251, θi = 18.21°), and this difference using MIMICS is 5.1 dB for October 29th (day 296, θi = 42.07°).

In figure 12, values lower than -17 dB in the simulations correspond to the radar signal in the dry season and incident angles higher than 30º. The main contribution to the radar backscatter for this season comes from the soil (see figures. 8 - 9). We note that the high errors are attributed to the low values of the soil moisture contents which are lower than 2%. In this case the scattering from soil is not necessarily all from surface roughness. Once the soil is dry the signal can penetrate deep and scattering from volumetric soil inhomogeneities can dominate.

6. Soil moisture content dependence

Because of the significance of soil contribution at low incidence angles, we study the relationship between the backscattering coefficient from the Sahelian grassland and soil moisture content.

Different experimental studies (Ulaby et al. 1986, Quesney et al. 2000) have shown that soil-moisture effect on the radar signal is approximately linear for values ranged between 35% and 40%. In (Zribi and Dechambre 2003), it is also observed that the IEM model keeps this linear behaviour for values ranging from 5% to 20%, independent of the roughness. Figure 13 illustrates the radar signal predicted by IEM as a function of the soil moisture content for the range of 0.1% to 12.3% and for a roughness of $h_{rms} = 8.5\,mm$ and $l_c = 274\,mm$ ($Z_s = 0.264\,mm$), which are values corresponding to the Sahelian grassland. From this figure, it is possible to conclude that for low moisture values (lower than 2%) this linear behaviour is no longer preserved.

Figure 14 shows the simulated backscattering coefficient and ENVISAT ASAR data normalized at 23° in function of soil moisture content for Agoufou. To normalize the ENVISAT data the hybrid method proposed in (Monsivais-Huertero et al. 2006) is used. This hybrid method let us consider not only the soil effect but also the vegetation one on the radar signal. In this paper we change a step of that procedure: instead of taking the soil contribution equal to ENVISAT data at HH polarization during dry season, it is calculated using the IEM model. Comparing the two curves for low values of moisture (lower than 2%) it is obvious that neither follow a linear behaviour. Furthermore, normalized data present a high dispersion for this range of values. For values higher than 2%, the linear behaviour is obtained.

Considering the entire range influential parameters, the correlation coefficient between simulations and soil moisture content is equal to r = 0.88. For the case of normalized data (Monsivais-Huertero et al. 2006), the correlation coefficient is r = 0.55.

According to these correlation coefficients, it is not possible to estimate soil moisture with enough accuracy from the HH backscatter at 23° if one assumes the entire backscatter comes only from the soil surface.

7. Conclusion and future works

In this paper we compare the radar response obtained by the three microwave scattering models to understand and predict the dynamic of the Sahelian grassland. Two models are based on a coherent formulation, one uses the specific generator for the African grassland and the second one considers a random generator. The third model is based on the Radiative Transfer theory (incoherent formulation). The three models calculate the contribution for each type of scatterers: shrubs, grass and soil. To validate the models, we use ENVISAT ASAR data collected in 2005.

From the comparative analysis of the two coherent formulations using different generators, the following remarks can be pointed out:

1. Both two models get similar levels of backscattering coefficient due to compensation in the different contributions.

2. For grass, it is observed an inversion in the main contributor for HH polarization at 40° and HV polarization at 23° and 40°.

3. For shrubs, both two models predict the same main contributions. In all cases, the double scattering is higher than the direct scattering.

From the comparative analysis of the two formulations (coherent and incoherent), the following points can be concluded:

1. For grass, the level of direct scattering is lower than that of double scattering according to the coherent model, whereas the incoherent formulation predicts opposite behaviour.

2. For shrubs, also opposite behaviour between the two models is observed at VV polarization. At HH and HV polarizations, both two models obtain the same behaviour, even though the difference between the double scattering and the direct scattering is higher in the coherent model.

With the exception of 40° at HH polarization, predicted curves depict a significant dependence on the soil contribution. For the case of 40° at HH polarization, the main contribution comes from grass for the coherent formulation. The radar signal shows the different stages of grass growth during the rainy season. The grass contribution is dominated by the double scattering at VV and HH polarizations when considering a coherent formulation and the plant structure.

The formulation which matches the best with ENVISAT data is the coherent formulation considering the plant structure (correlation = 0.92). At the time of this study, only data at HH polarization were available, therefore a validation on VV polarization should be carried out in future works.

Errors in this modelling can be attributed to assumptions made and lack of ancillary data. The study of the relationship between radar signal and soil moisture content shows that for low moisture content values, the linear behaviour mentioned in previous works (Zribi and Dechambre 2003, Ulaby et al. 1986, Quesney 2000) is not valid. For values higher than 2%, this linear relationship is kept and allows us to propose an empirical equation for predicting the radar backscatter as a function of soil moisture.

Acknowledgment

Authors would sincerely thank to Dr. Mehrez Zribi of CETP (Centre d'Etude des Environnements Terrestre et Planétaires, Paris, France) for providing us an incoherent version of the IEM model to carry out the soil modelling and for his helpful advices. We would also like to thank Dr. Eric Mougin and Dr. Frédéric Baup of CESBIO (Centre d'Etudes Spatiales de la

Biosphère) for supplying us with ground data collected during the campaign of 2005 and their interest in this research.

A. Monsivais-Huertero was supported by a scholarship of the Mexican Council of Science and Technology (CONACYT).

References

AMMA (African Monsoon Multidisciplinary Analysis), 2002, La Mousson Ouest Africaine et ses Composantes, White book, Available: http://amma.mediasfrance.org/france/ (accessed 4 June 2007)

BAKHTIARI, S. and ZOUGHI, R., 1991, A model for backscattering characteristics of tall prairie grass canopies at microwave frequencies, *Remote Sensing of Environment*, **36**, 137-147.

BAUP F., MOUGIN E., HIERNAUX P., LOPES A., DE ROSNAY P., CHÊNERIE I., 2007, Signatures of Sahelian surfaces in Mali using ENVISAT-ASAR data, *IEEE Transaction on Geoscience and Remote Sensing*, **45 (7)**, 2354-2363.

BEAUCHEMIN, M., THOMSON, K. P. B., and EDWARDS, G., 1995, Modelling forest stands with MIMICs: implications for calibration, *Canadian Journal of Remote Sensing*, **21**, 518-526.

BEST-Basic ENVISAT SAT Toolbox, User Manual, Version 4.0.2, Mar. 2005. Available: http://envisat.esa.int/services/best/documentation/ (accessed 4 June 2007)

BOUMAN, B. A. M., 1991, Crop parameter estimation from ground-based X-band (3-cm wave) radar backscattering data, *Remote Sensing of Environment*, **37**, 193-205.

CHEN, K. S., WU, T. D., TSAY, M. K., and FUNG, A. K., 2000, A note on the multiple scattering in an IEM model, *IEEE Trans. Geosci. Remote Sens.*, **38**, 249-256.

ESA (European Space Agency), 2004, *ENVISAT ASAR Product Handbook*, Issue 1.2.

FERRAZZOLI, P., PALOSCIA, S., PAMPALONI, P., SCHIAVON, G., SOLIMINI, D., and COPPO, P., 1992, Sensitivity of microwave measurements to vegetation biomass and soil moiture content: A case study, *IEEE Trans. Geosci. Remote Sens.*, **30**, 750-756.

FRISON, P. L., MOUGIN, E., and HIERNAUX, P., 1998, Observations and interpretation of seasonal ERS-1 wind scatterometer data over northern Sahel (Mali), *Remote Sensing of Environment*, **63**, 233-242.

FRISON, P. L., MOUGIN, E., JARLAN, L., KARAM, M. A., and HIERNAUX, P., 2000, Comparison of ERS wind-scatterometer and SSM/I data for Sahelian vegetation monitoring, *IEEE Trans. Geosci. Remote Sens.*, **38**, 1794-1803.

FUNG, A. K., 1994, *Microwave Scattering and Emission Models and their Applications* (Boston, MA: Artech House).

FUNG, A. K., LI, Z., and CHEN, K. S., 1992, Backscattering from a randomly rough dielectric surface, *IEEE Trans. Geosci. Remote Sens.*, **30**, 356-369.

GASKIN, G. J. and MILLER, J. D., 1996, Measurements of soil water content using a simplified impedance measuring technique, *Journal of Agricultural Engineering Resources*, **63**, 153-160.

HSIEH, C. Y., FUNG, A. K., NESTI, G., SIEBER, A. J., and COPPO, P., 1997, A further study of the IEM surface scattering model, *IEEE Trans. Geosci. Remote Sens.*, **35**, 901-909.

JARLAN, L., MOUGIN, E., FRISON, P. L., MAZZEGA, P., and HIERNAUX, P., 2002, Analysis of ERS wind scatterometer time series over Sahel (Mali), *Remote Sensing of Environment*, **81**, 404-415.

KARAM, M. A. and FUNG, A. K., 1989, Leaf-shape effects in electromagnetic wave scattering from vegetation, *IEEE Trans. Geosci. Remote Sens.*, **27**, 687-697.

LIANG, P., MOGHADDAM, M., PIERCE, L. E., and LUCAS, R. M., 2005, Radar backscattering model for multilayer mixed-species forests, *IEEE Trans. Geosci. Remote Sens.*, **43**, 2612-2626.

LIANG, P., PIERCE, L. E., and MOGHADDAM, M., 2005bis, Radiative transfer model for microwave bistatic scattering from forest canopies, *IEEE Trans. Geosci. Remote Sens.*, **43**, 2470-2483.

MCDONALD, K. C. and ULABY, F. T., 1993, Radiative transfer modelling of discontinuous tree canopies at microwave frequencies, *Int. J. Remote Sens.*, **14**, 2097-2128.

MCDONALD, K., DOBSON, M., and ULABY, F., 1990, Using MIMICS to model L-band multiangle and multitemporal backscatter from a walnut orchard, *IEEE Trans. Geosci. Remote Sens.*, **28**, 477-491.

MONSIVAIS-HUERTERO, A., CHENERIE, I., BAUP, F., MOUGIN, E., and SARABANDI, K., 2006, Angular normalization of ENVISAT ASAR data over Sahelian-grassland using a coherent scattering model, in *Proc. PIERS 2006 Cambridge*, 2006, (The Electromagnetics Academy: Cambridge, MA, USA), 94-98.

MONSIVAIS-HUERTERO, A., CHENERIE, I., and SARABANDI, K., 2007, Scattering from Sahelian grassland: A coherent modeling, in *Proc. IGARSS 2007*, (IEEE International Geoscience and Remote Sensing Symposium), 2543-2545.

MOUGIN, E., LO SEEN, D., RAMBAL, S., GASTON, A., and HIERNAUX, P., 1995, A regional sahelian grassland model to be coupled with multispectral satellite data. I. Description and validation, *Remote Sensing of Environment*, **52**, 181-193.

OGILVY, O., 1991, *Theory of Wave Scattering from Random Rough Surfaces* (Bristol: Adam Hilder).

PEPLINSKI, N. R., ULABY, F. T., and DOBSON, M. C., 1995, Dielectric properties of soils in the 0.3-1.3 GHz range, *IEEE Trans. Geosci. Remote Sens.*, **33**, 803-807.

PICARD, G., LE TOAN, T., and MATTIA, F., 2003, Understanding C-band backscatter from wheat canopy using a multiple-scattering coherent model, *IEEE Trans. Geosci. Remote Sens.*, **41**, 1583-1591.

QUESNEY, A., LE HÉGARAT-MASCLE, S., TACONNET, O., VIDAL-MADJAR, D., WIGNERON, J. P., LOUMAGNE, C., and NORMAND, M., 2000, Estimation of watershed soil moisture index from ERS/SAR data, *Remote Sensing of Environment*, **72**, 290-303.

RAKOTOARIVONY, L., TACONET, O., VIDAL-MADJAR, D., and BENALLEGUE, M., 1996, Radar backscattering over agricultural bare soils, *Journal of Electr. Waves Applic.*, **10**, 187-209.

SAATCHI, S. S., LE VINE, D. M., and LANG, R. H., 1994, Microwave backscattering and emission model for grass canopies, *IEEE Trans. Geosci. Remote Sens.*, **32**, 177-186.

SAATCHI, S. S. and MCDONALD, K. C., 1997, Coherent effects in microwave backscattering models for forest canopies, *IEEE Trans. Geosci. Remote Sens.*, **35 (4)**, 1032-1044.

STILES, J. M., SARABANDI, K., and ULABY, F. T., 1993, Microwave scattering model for grass blade structures, *IEEE Trans. Geosci. Remote Sens.*, **31**, 1051-1059.

STILES, J. M. and SARABANDI, K., 2000, Electromagnetic scattering from grassland – Part I: A fully phase-coherent scattering model, *IEEE Trans. Geosci. Remote Sens.*, **38**, 339-348.

STILES, J. M., SARABANDI, K., and ULABY, F. T., 2000, Electromagnetic scattering from grassland – Part II: Measurements and modeling results, *IEEE Trans. Geosci. Remote Sens.*, **38**, 349-356.

TACONET, O., BENALLEGUE, M., VIDAL-MADJAR, D., PREVOT, L., DECHAMBRE, M., and NORMAND, M., 1994, Estimation of soil and crop parameters for wheat from airbone radar backscattering data in C and X bands, *Remote Sensing of Environment*, **50**, 287-294.

THIRION, L., CHENERIE, I., and GALY, C., 2004, Application of a coherent model in simulating the backscattering coefficient of a mangrove forest, *Waves Random Media*, **14**, 393-414.

TOURÉ, A., THOMSON, K. P. B., EDWARDS, G., BROWN, R. J., and BRISCO, B. G., 1994, Adaptation of the MIMICS backscattering model to the agricultural context-wheat and canola at L and C bands, *IEEE Trans. Geosci. Remote Sens.*, **32**, 47-61.

TRACOL, Y., 2004, Etude des Variations Interannuelles de la Productions Herbacée des Pâturages Sahéliens: Exemple du Gourma Malien, Ph.D. thesis, Univ. Paul Sabatier, Toulouse, France.

TSANG, L., KONG, J., and SHIN, R., 1985, *Theory of Microwave Remote Sensing* (New York: Wiley).

ULABY, F. T., MORE, R. K., and FUNG, A. K., 1986, *Microwave Remote Sensing: Active and Passive*. Vol. II (Boston, MA:Artech House) 922-973

ULABY, F., SARABANDI, K., MCDONALD, K., WHITT, M., and DOBSON, M., 1988, Michigan Microwave Canopy Scattering Model (MIMICS), *Int. J. Remote Sens*., **12**, 1123-1153.

ULABY, F.and EL –RAYES, M. A., 1987, Microwave dielectric spectrum of vegetation, Part II: Dual-dispersion model, *IEEE Trans. Geosci. Remote Sens.*, **GE-25**, 550-557.

ULABY, F.and ELACHI, C., 1990, *Radar Polarimetry for Geoscience Applications* (Norwood, MA: Arthec House).

WHITE, R. P. and NACKONEY, J., 2002, Drylands, People, and Ecosystem Goods and Services: A Web-based Geospatial Analysis, WRI. Available online at: http://biodiv.wri.org/pubs_description.cfm?PubID=3813 (accessed 4 June 2007)

WU, T. D., CHEN, K. S., SHI, J., and FUNG, A. K., 2001, A transition model for the reflection coefficient in surface scattering, *IEEE Trans. Geosci. Remote Sens.*, **39**, 2040-2050.

ZRIBI, M. and DECHAMBRE, M., 2003, A new empirical model to retrieve soil moisture and roughness from C-band radar data, *Remote Sensing of Environment*, **84**, 42-52.

ZRIBI, M., CIARLETTI, V., and TACONET, O., 2000, Validation of a Rough Surface Model Based on Fractional Brownian Geometry with SIRC and ERASME Radar Data over Orgeval, *Remote Sensing of Environment*, **73**, 65-72.

ZRIBI, M., TACONET, O., LE HÉGARAT-MASCLE, S., VIDAL-MADJAR, D., EMBLANCH, C., LOUMAGNE, C., and NORMAND, M., 1997, Backscattering behavior and simulation comparison over bare soils using SIR-C/X-SAR and ERASME 1994 data over Orgeval, *Remote Sensing of Environment*, **59**, 256-266.

Table I. Tree description

Layer	Layer height (m)	Vegetal scatterer	Height (m)	Diameter (cm)	Density (m^{-3})	orientation	
						θ_t (°)	ϕ_t (°)
1 (bottom)	0.15	Trunk	0.15	5	0.04	0-30	0-30
2	0.65	Branch	0.65	4	0.036	0-30	0-30
3	0.60	Branch	0.60	2.5	0.098	0-35	0-50
4 (top)	0.60	Branch	0.60	1.76	0.05	0-35	0-50

Table II. Grass description

Parameter	Value
semi-major axis (cm)	10
semi-minor axis (cm)	0.3
thickness (cm)	0.03
orientation α (°)	0 – 360 (uniform distribution)
orientation β (°)	0 – 35 (erecthopile distribution)
orientation γ (°)	40 – 50 (uniform distribution)

Table III. Ancillary data.
Herb height, herb phytomass and herb density were obtained by using the step model (Mougin et al. 1995).

Date	Day	Air temperature (°C)	Herb gravimetric moisture	Herb height (m)	Herbaceous phytomass (kg/ha)	Herb density (m^{-3})	Soil moisture content (%)
30-May-2005	150	38.66					0.60
16-Jun-2005	167	35.66					1.62
21- Jun -2005	172	31.00					10.95
06- Jul -2005	187	35.93					3.15
16- Jul -2005	197	29.8	0.54	0.24	493	2215	5.85
29- Jul -2005	210	28.8	0.49	0.35	953	2862	1.60
01-Aug-2005	213	28.5	0.48	0.35	1030	3043	8.96
05-Aug-2005	217	29.9	0.47	0.36	1232	3512	2.68
14-Aug-2005	226	27.7	0.44	0.36	1691	4698	3.43
17-Aug-2005	229	25.7	0.43	0.36	1743	4805	9.30
20-Aug-2005	232	25.5	0.42	0.36	1845	5048	12.26
02-Sep-2005	245	31.00	0.36	0.36	2172	5698	6.45
03-Sep-2005	246	31.00	0.36	0.36	2120	5538	2.01
05-Sep-2005	248	28.00	0.34	0.36	2021	5233	1.64
06-Sep-2005	249	28.00	0.43	0.36	1971	5080	1.23
08-Sep-2005	251	28.00	0.32	0.36	1875	4832	1.28
09-Sep-2005	252	29.00	0.32	0.34	1826	4926	1.04
18-Sep-2005	261	32.00	0.26	0.05	1395	24893	0.89
21-Sep-2005	264	30.00	0.24	0.047	1303	24430	0.77
22-Sep-2005	265	30.00	0.23	0.047	1274	25298	3.78

24-Sep-2005	267	31.00	0.22	0.047	1221	22681	1.32
25-Sep-2005	268	31.00	0.21	0.047	1196	22137	0.78
07-Oct-2005	280	31.00	0.14	0.047	944	16866	7.04
08-Oct-2005	281	31.00	0.13	0.047	927	16511	3.73
10-Oct-2005	283	31.00	0.12	0.047	893	15828	2.42
14-Oct-2005	287	31.00	0.09	0.047	830	14554	1.13
23-Oct-2005	296	31.00	0.05	0.047	707	12190	0.82
27-Oct-2005	300	30.79					0.79
11-Nov-2005	315	29.92					0.57
16-Nov-2005	320	29.48					0.58

Table IV. Geometrical parameters for the grass structures.

		Seedling				**Adult plant**				**Dry plant**			
	Category	**l (cm)**	**r (cm)**	**α (°)**	**β (°)**	**l (cm)**	**r (cm)**	**α (°)**	**β (°)**	**l (cm)**	**r (cm)**	**α (°)**	**β (°)**
Stalks	**1**	4.8	0.5	0	0	7.2	0.5	0	60	1	0.5	0	60
	2	2.4	0.5	0	0	4.05	0.5	0	30	0.56	0.5	0	30
	3	7.2	0.5	0	0	20.7	0.5	180	10	2.88	0.5	180	10
Blades	**1**	9.6		0	35	3.6		0	70	0.5		0	70
	2	4.8		180	35	16.2		180	10	4.5		180	10
	3	4.8		180	35	8.1		180	155	2.26		180	155
	4	4.8		0	35	2.7		0	45	0.72		0	45
	5	4.8		0	35	18		0	10	5		0	10
	6	9.6		120	35	21.6		120	30	6		120	30
	7	9.6		0	35	10.8		0	30	3		0	30
	8	9.6		240	35	16.2		240	30	2.5		240	30

Table V. ENVISAT-ASAR data

Date	Day	Incidence angle (°)	$\sigma^0(\mathrm{dB})$	Orbit	Polarization
16-Jan-2005	16	42.10	-16.84	descending	V/V
04-Feb-2005	35	38.09	-16.77	descending	V/V
23-Feb-2005	54	33.72	-16.35	descending	V/V
26-Feb-2005	57	23.79	-13.40	descending	V/V
30-Mar-2005	89	33.73	-16.28	descending	V/V
15-Apr-2005	105	38.06	-16.88	descending	V/V
18-Apr-2005	108	28.88	-15.61	descending	V/V
23-May-2005	143	28.91	-16.88	descending	V/V
05-Jun-2005	156	42.12	-16.45	descending	V/V
16-Jul-2005	197	23.71	-12.01	descending	H/H
29-Jul-2005	210	38.07	-15.92	descending	H/H
01-Aug-2005	213	28.91	-12.03	descending	H/H
05-Aug-2005	217	39.98	-13.75	ascending	H/H
14-Aug-2005	226	42.12	-14.41	descending	H/H
17-Aug-2005	229	33.70	-12.21	descending	H/H
20-Aug-2005	232	23.77	-9.78	descending	H/H
02-Sep-2005	245	38.06	-14.57	descending	H/H
03-Sep-2005	246	20.89	-12.45	ascending	H/H
05-Sep-2005	248	28.88	-15.58	descending	H/H
06-Sep-2005	249	31.21	-15.09	ascending	H/H
08-Sep-2005	251	18.21	-13.50	descending	H/H
09-Sep-2005	252	40.06	-16.44	ascending	H/H
18-Sep-2005	261	42.08	-16.10	descending	H/H
21-Sep-2005	264	33.67	-17.16	descending	H/H
22-Sep-2005	265	26.26	-12.83	ascending	H/H
24-Sep-2005	267	23.74	-13.47	descending	H/H
25-Sep-2005	268	35.82	-16.39	ascending	H/H
07-Oct-2005	280	38.09	-15.53	descending	H/H
08-Oct-2005	281	20.88	-12.19	ascending	H/H
10-Oct-2005	283	28.91	-15.40	descending	H/H
14-Oct-2005	287	40.03	-17.01	ascending	H/H

23-Oct-2005	296	42.07	-16.87	descending	H/H

Table VI. Major contribution predicted by the coherent model with a specific generator (Monsivais et al. 2007) and the coherent model with a uniform-distribution generator (Thirion et al. 2004).

Polarization	Incidence angle	Coherent model with a specific generator	Coherent model with a uniform-distribution generator
VV	23°	Direct scattering from soil	Direct scattering from soil
	40°	Direct scattering from soil	Direct scattering from soil
HH	23°	Direct scattering from soil	Direct scattering from soil
	40°	Double scattering from grass	Direct scattering from soil and both direct and double scatterings from grass
HV	23°	Double scattering from grass	Direct scattering from grass
	40°	Double scattering from grass	Direct scattering from grass

Table VII. Dynamics shown by the coherent model with a specific generator and by the coherent model with a uniform-distribution generator.

	Coherent model with a specific generator		Coherent model with a uniform-distribution generator	
	23°	**40°**	**23°**	**40°**
$\sigma^0_{VV}(\mathrm{dB})$	4.78	5.64	5.18	5.61
$\sigma^0_{HH}(\mathrm{dB})$	5.27	9.22	5.47	8.31
$\sigma^0_{HV}(\mathrm{dB})$	22.78	20.45	18.84	16.12

Table VIII. Major contribution predicted by the coherent model with a specific generator (Monsivais et al. 2007) and MIMICS (Ulaby et al. 1988).

Polarization	Incidence angle	Coherent model with a specific generator	MIMICS
VV	23°	Direct scattering from soil	Direct scattering from soil
	40°	Direct scattering from soil	Direct scattering from soil
HH	23°	Direct scattering from soil	Direct scattering from soil
	40°	Double scattering from grass	Direct scattering from soil
HV	23°	Double scattering from grass	Direct and double scattering from shrub
	40°	Double scattering from grass	Direct and double scattering from shrub

Table IX. Dynamics shown by the coherent model with a specific generator and by MIMICS.

	Coherent model with a specific generator		MIMICS	
	23°	40°	23°	40°
$\sigma^0_{VV}(\mathrm{dB})$	4.78	5.64	5.15	5.44
$\sigma^0_{HH}(\mathrm{dB})$	5.27	9.22	4.62	4.35
$\sigma^0_{HV}(\mathrm{dB})$	22.78	20.45	3.43	3.00

LIST OF FIGURES

FIGURE 1

(a)

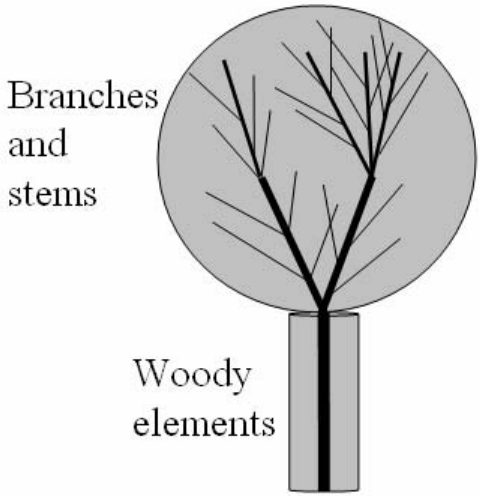

(b)

(c)

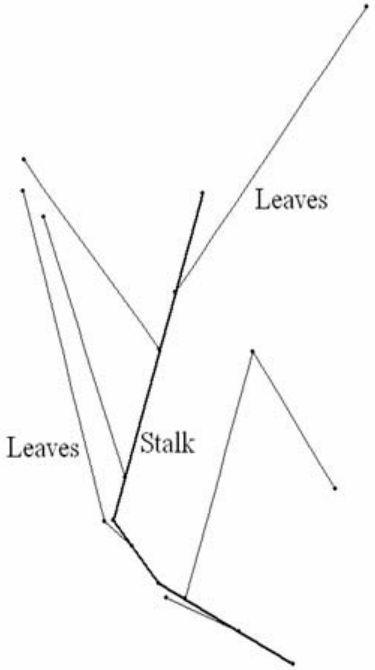

(d)

FIGURE 2

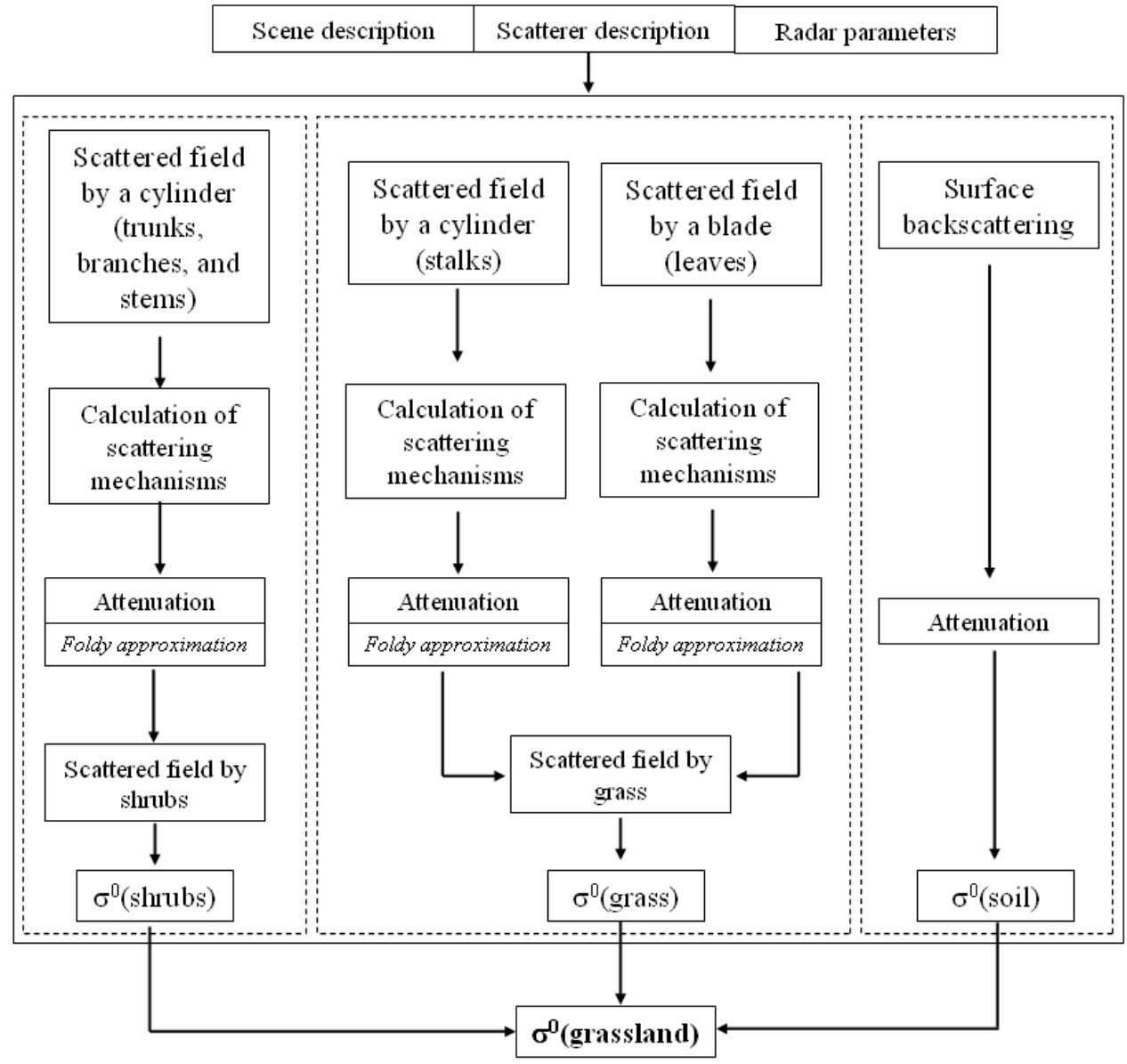
Scene description
Scatterer description
Radar parameters
Scattered field by a cylinder (trunks, branches, and stems)
Calculation of scattering mechanisms
Attenuation
Foldy approximation
Scattered field by shrubs
σ0(shrubs)
Scattered field by a cylinder (stalks)
Calculation of scattering mechanisms
Attenuation
Foldy approximation
Scattered field by a blade (leaves)
Calculation of scattering mechanisms
Attenuation
Foldy approximation
Scattered field by grass
σ0(grass)
Surface backscattering
Attenuation
σ0(soil)
σ0(grassland)

FIGURE 3

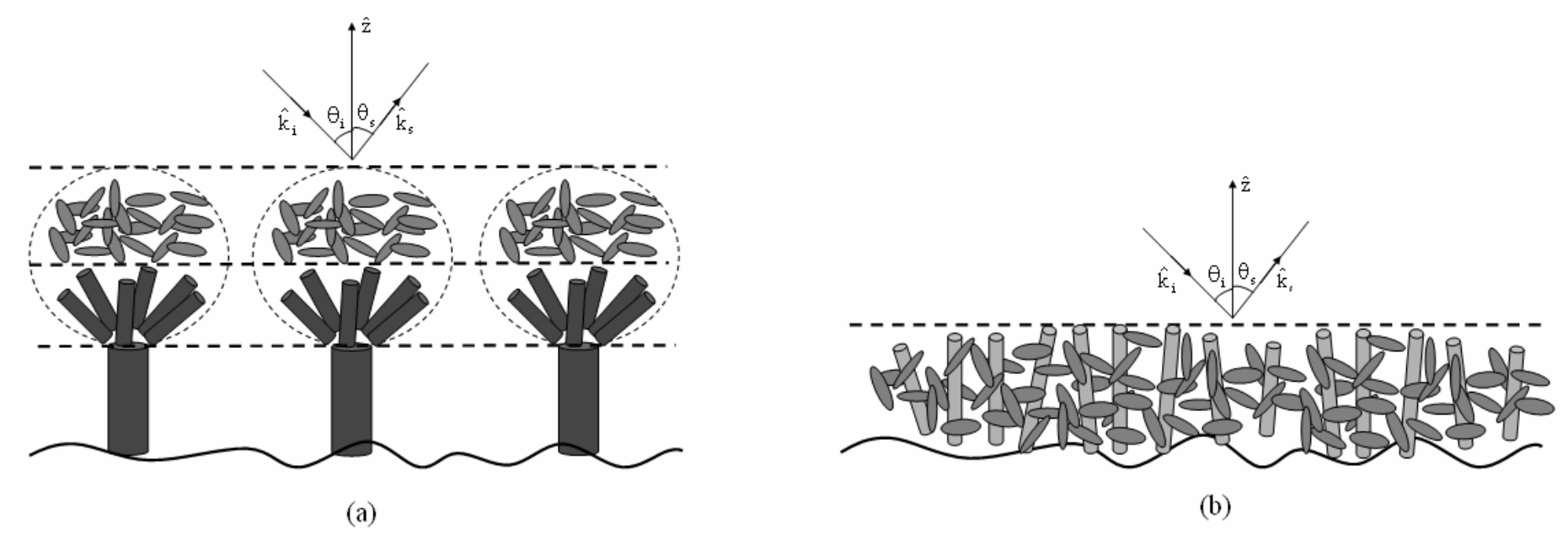

FIGURE 4

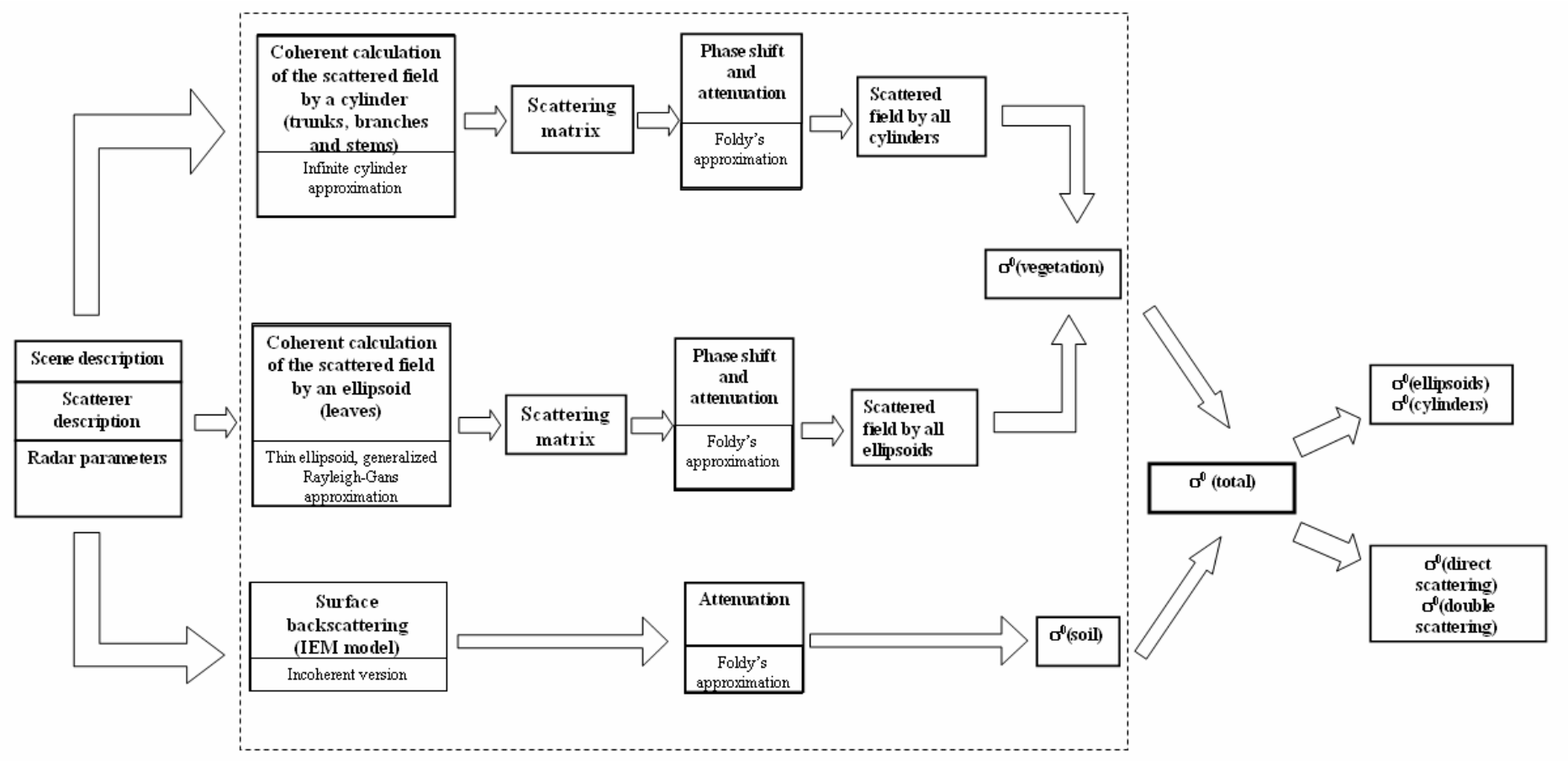
Scene description
Scatterer description
Radar parameters
Coherent calculation of the scattered field by a cylinder (trunks, branches and stems)
Infinite cylinder approximation
Scattering matrix
Phase shift and attenuation
Foldy's approximation
Scattered field by all cylinders
σ⁰(vegetation)
Coherent calculation of the scattered field by an ellipsoid (leaves)
Thin ellipsoid, generalized Rayleigh-Gans approximation
Scattering matrix
Phase shift and attenuation
Foldy's approximation
Scattered field by all ellipsoids
Surface backscattering (IEM model)
Incoherent version
Attenuation
Foldy's approximation
σ⁰(soil)
σ⁰ (total)
σ⁰(ellipsoids)
σ⁰(cylinders)
σ⁰(direct scattering)
σ⁰(double scattering)

FIGURE 5

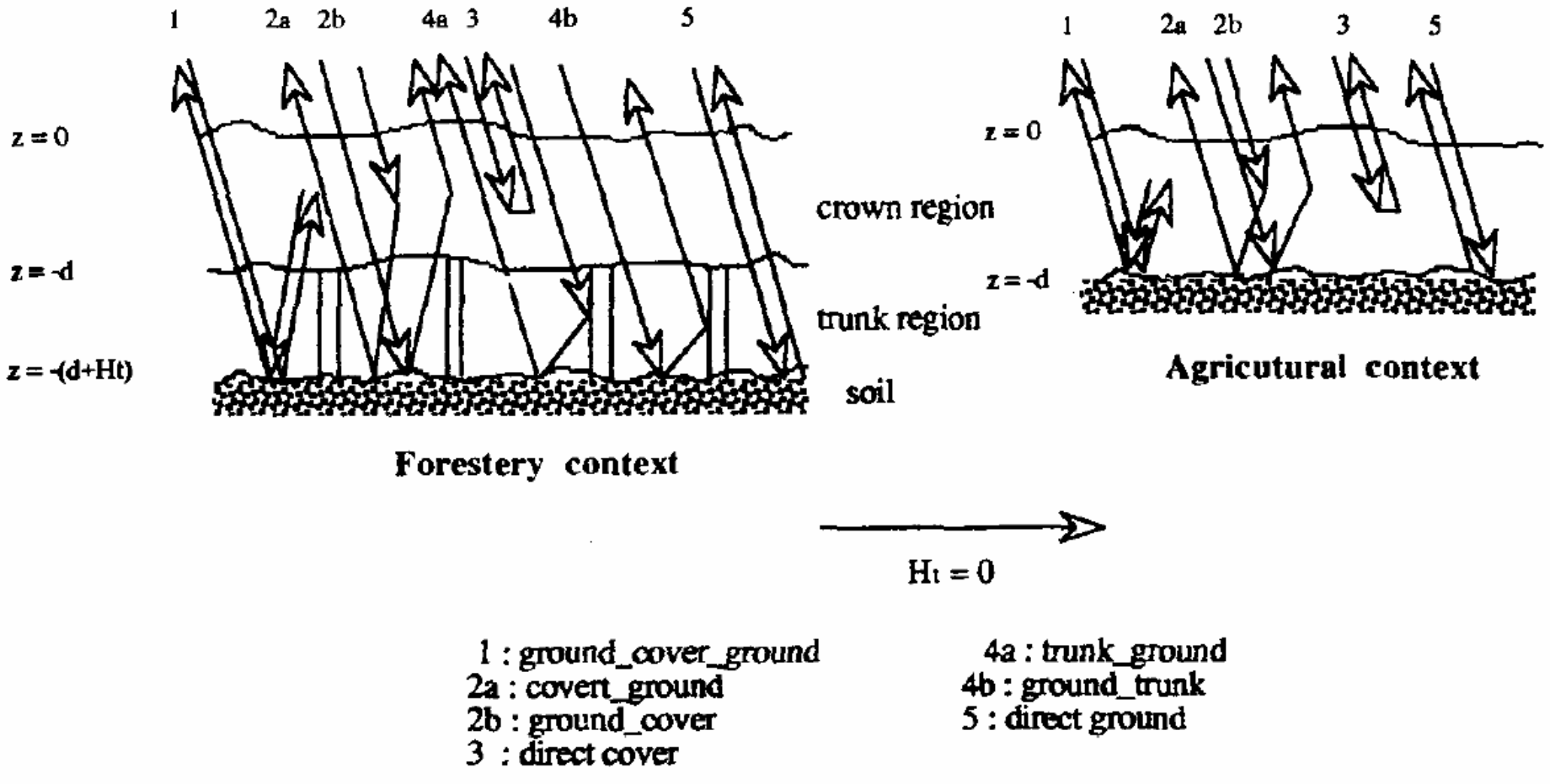
1
2a
2b
4a
3
4b
5
z = 0
z = -d
z = -(d+Ht)
crown region
trunk region
soil
Forestery context
1
2a
2b
3
5
z = 0
z = -d
Agricutural context
Ht = 0
1 : ground_cover_ground
2a : covert_ground
2b : ground_cover
3 : direct cover
4a : trunk_ground
4b : ground_trunk
5 : direct ground

FIGURE 6

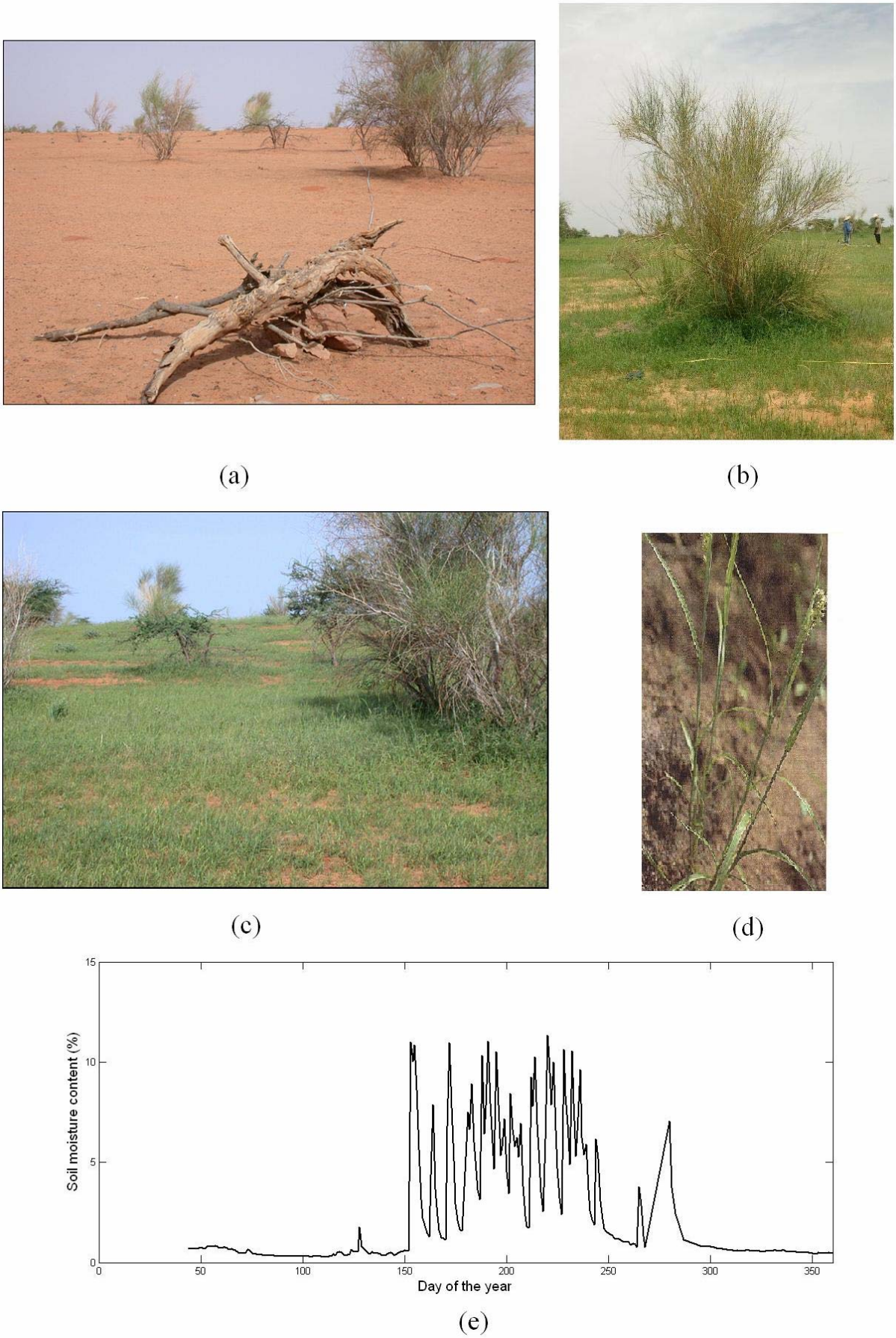
(a)
(b)
(c)
(d)
Soil moisture content (%)
Day of the year
0
5
10
15
0
50
100
150
200
250
300
350
(e)

FIGURE 7

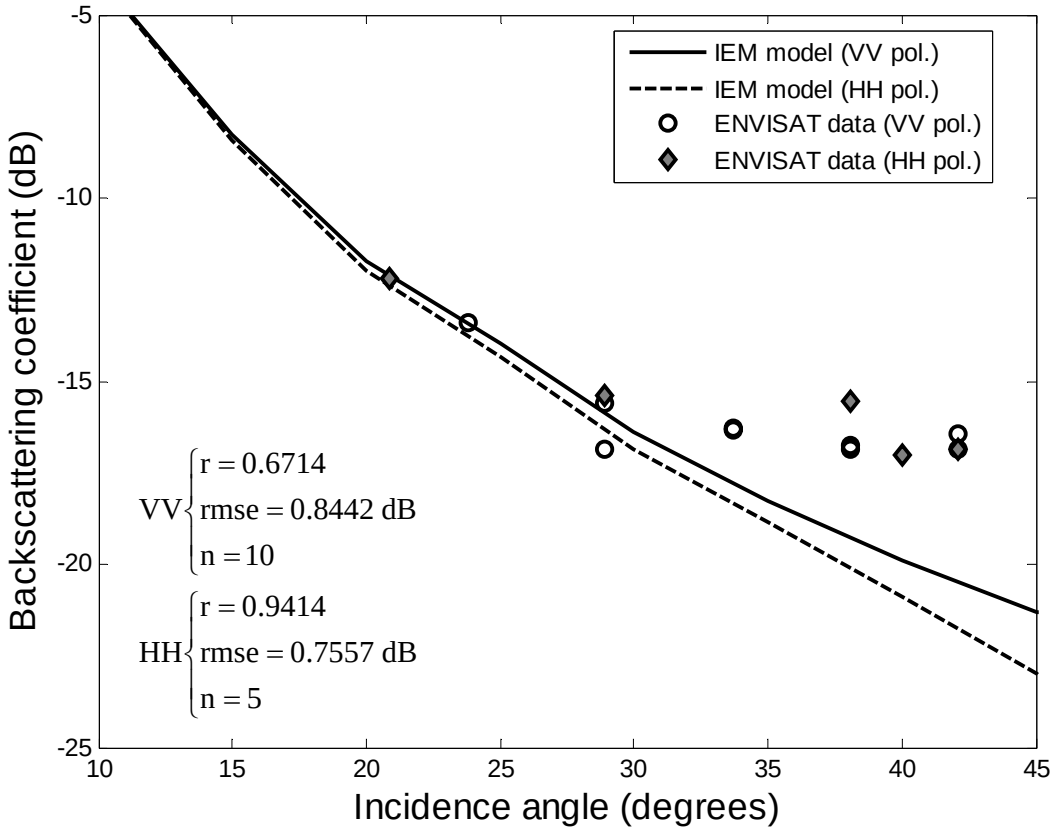
IEM model (VV pol.)
IEM model (HH pol.)
ENVISAT data (VV pol.)
ENVISAT data (HH pol.)
VV
r = 0.6714
rmse = 0.8442 dB
n = 10
HH
r = 0.9414
rmse = 0.7557 dB
n = 5
Backscattering coefficient (dB)
Incidence angle (degrees)
-5
-10
-15
-20
-25
10
15
20
25
30
35
40
45

FIGURE 8

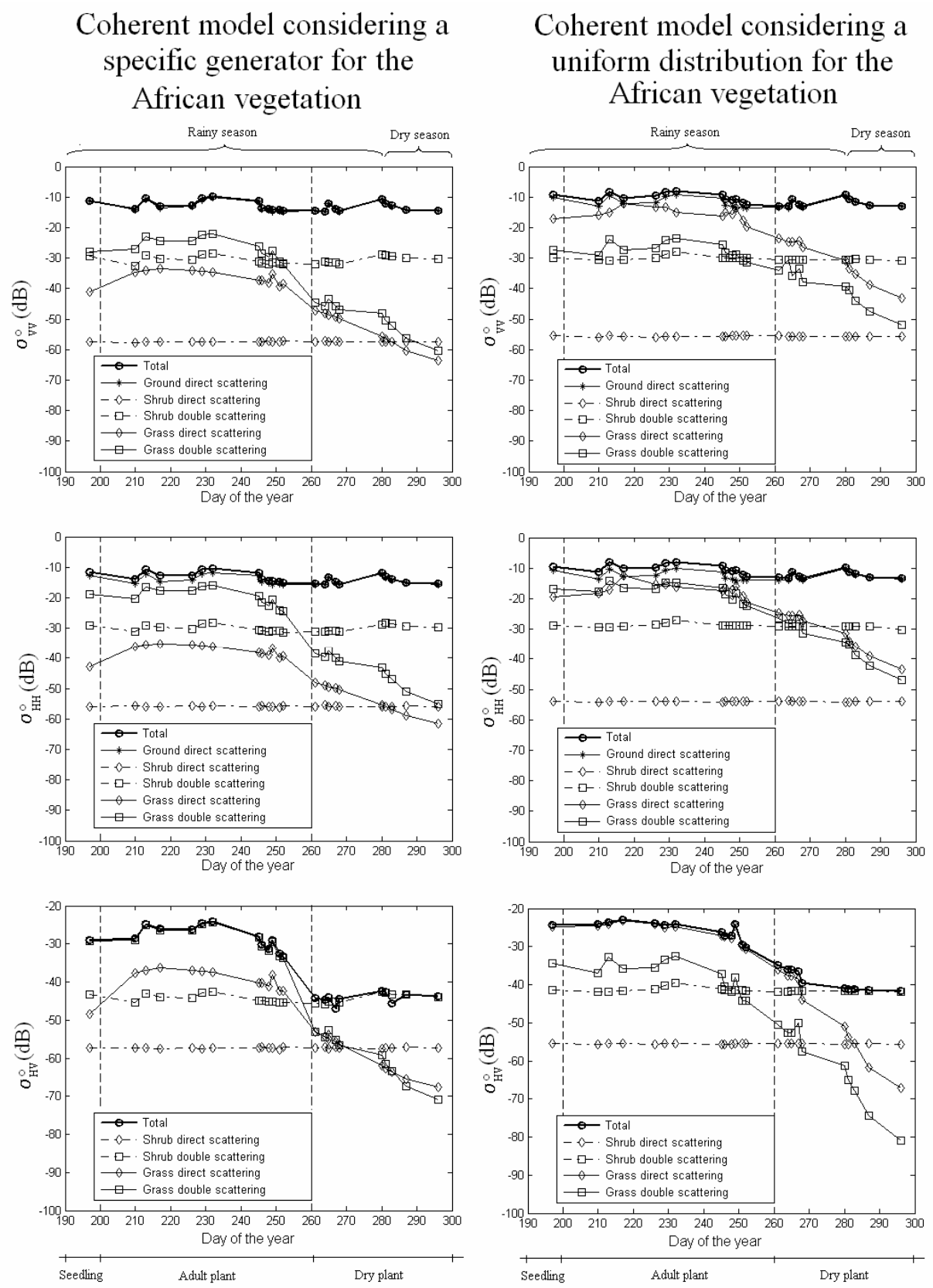
Coherent model considering a specific generator for the African vegetation
Coherent model considering a uniform distribution for the African vegetation
Rainy season
Dry season
σ°_{VV} (dB)
σ°_{HH} (dB)
σ°_{HV} (dB)
Day of the year
Total
Ground direct scattering
Shrub direct scattering
Shrub double scattering
Grass direct scattering
Grass double scattering
Seedling
Adult plant
Dry plant

FIGURE 9

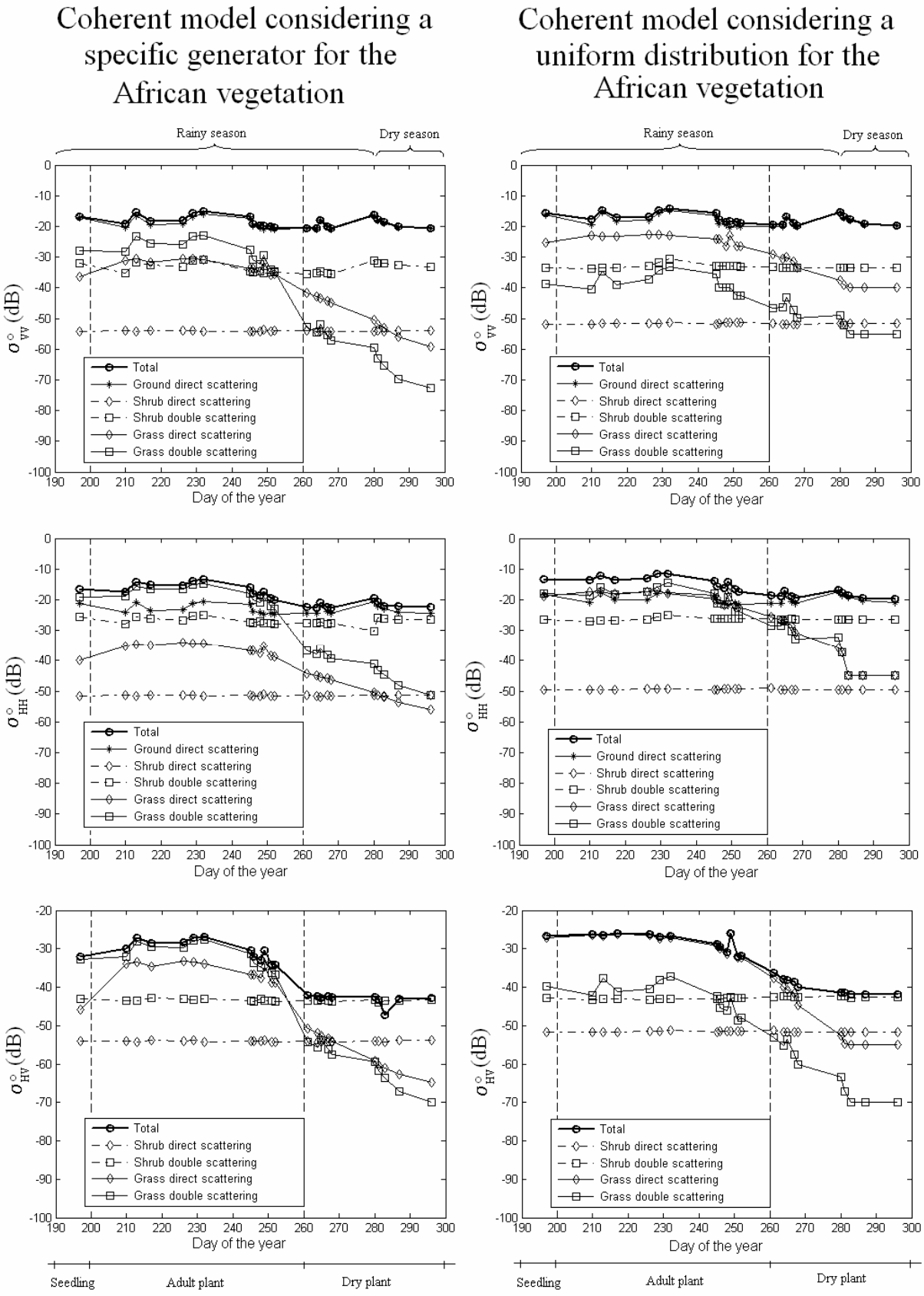
Coherent model considering a specific generator for the African vegetation
Coherent model considering a uniform distribution for the African vegetation
Rainy season
Dry season
σ°_{VV} (dB)
σ°_{HH} (dB)
σ°_{HV} (dB)
Day of the year
Total
Ground direct scattering
Shrub direct scattering
Shrub double scattering
Grass direct scattering
Grass double scattering
Seedling
Adult plant
Dry plant

FIGURE 10

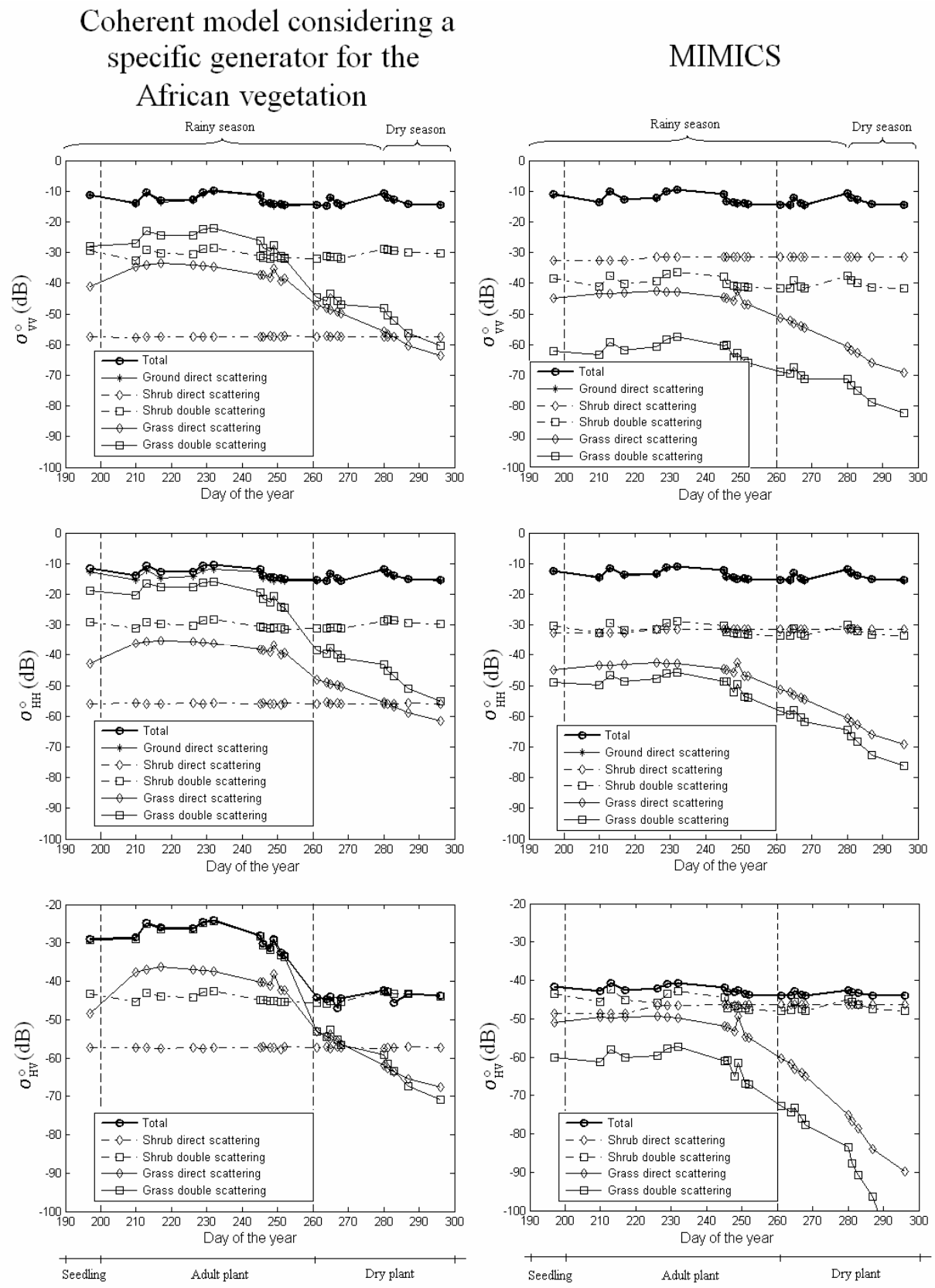
Coherent model considering a specific generator for the African vegetation
MIMICS
Rainy season
Dry season
σ°_{VV} (dB)
σ°_{HH} (dB)
σ°_{HV} (dB)
Day of the year
Total
Ground direct scattering
Shrub direct scattering
Shrub double scattering
Grass direct scattering
Grass double scattering
Seedling
Adult plant
Dry plant

FIGURE 11

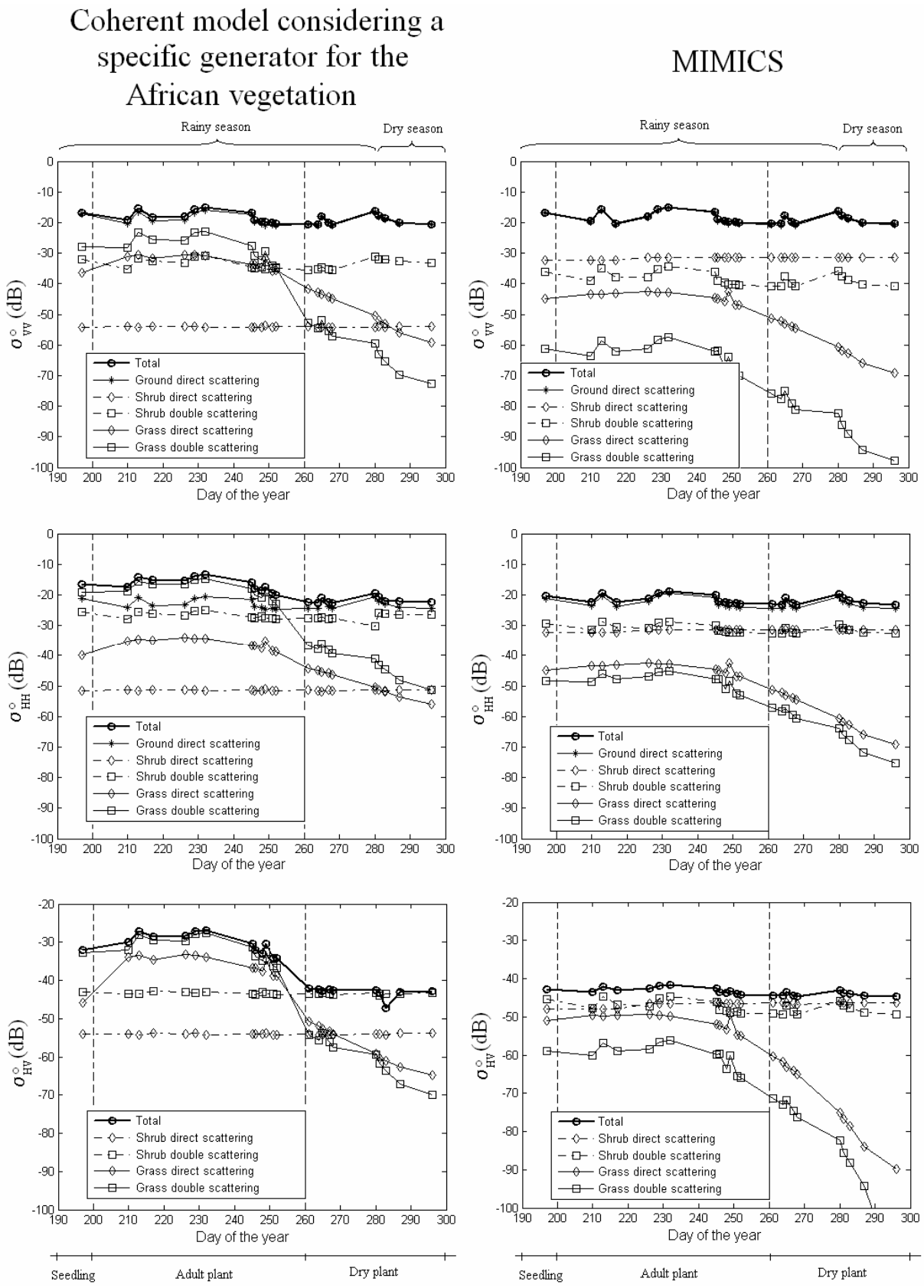
Coherent model considering a specific generator for the African vegetation
MIMICS
Rainy season
Dry season
σ°_{VV} (dB)
σ°_{HH} (dB)
σ°_{HV} (dB)
Total
Ground direct scattering
Shrub direct scattering
Shrub double scattering
Grass direct scattering
Grass double scattering
Day of the year
Seedling
Adult plant
Dry plant

FIGURE 12

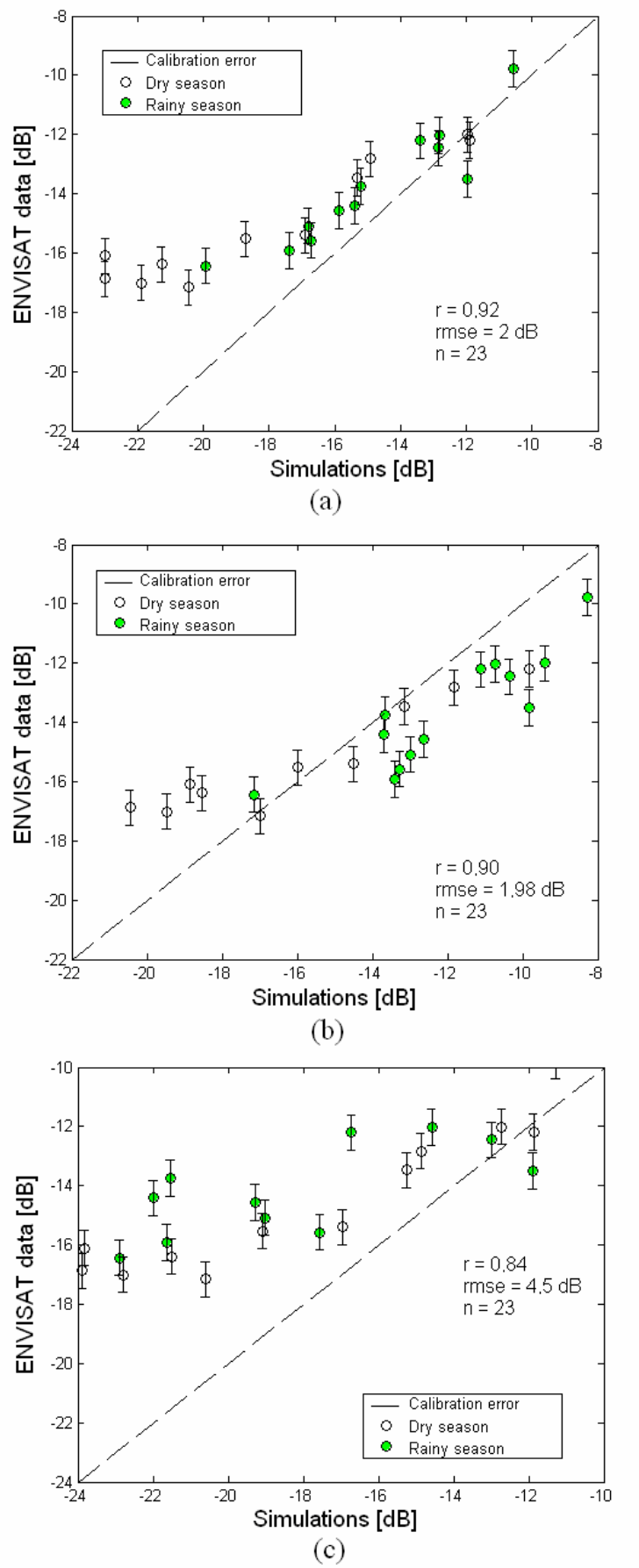
Calibration error
Dry season
Rainy season
ENVISAT data [dB]
Simulations [dB]
r = 0,92
rmse = 2 dB
n = 23
(a)
Calibration error
Dry season
Rainy season
ENVISAT data [dB]
Simulations [dB]
r = 0,90
rmse = 1,98 dB
n = 23
(b)
Calibration error
Dry season
Rainy season
ENVISAT data [dB]
Simulations [dB]
r = 0,84
rmse = 4,5 dB
n = 23
(c)

FIGURE 13

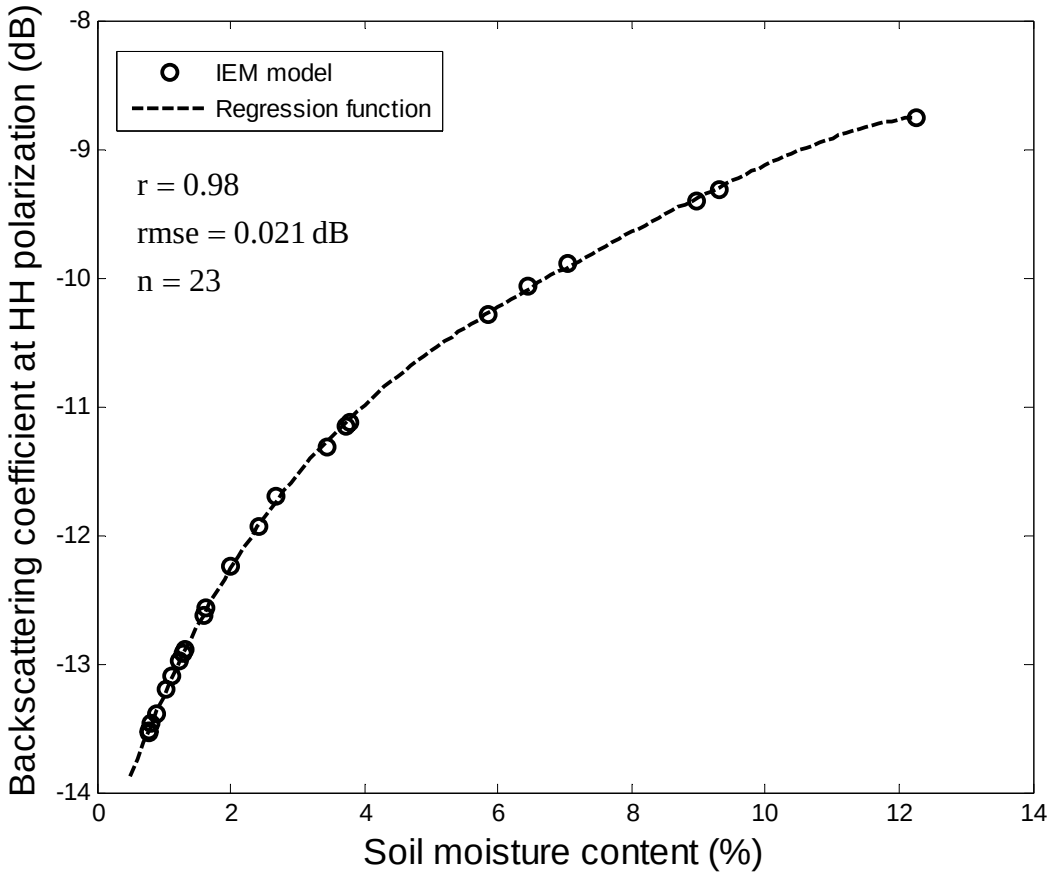
IEM model
Regression function
r = 0.98
rmse = 0.021 dB
n = 23
Backscattering coefficient at HH polarization (dB)
Soil moisture content (%)
-8
-9
-10
-11
-12
-13
-14
0
2
4
6
8
10
12
14

FIGURE 14

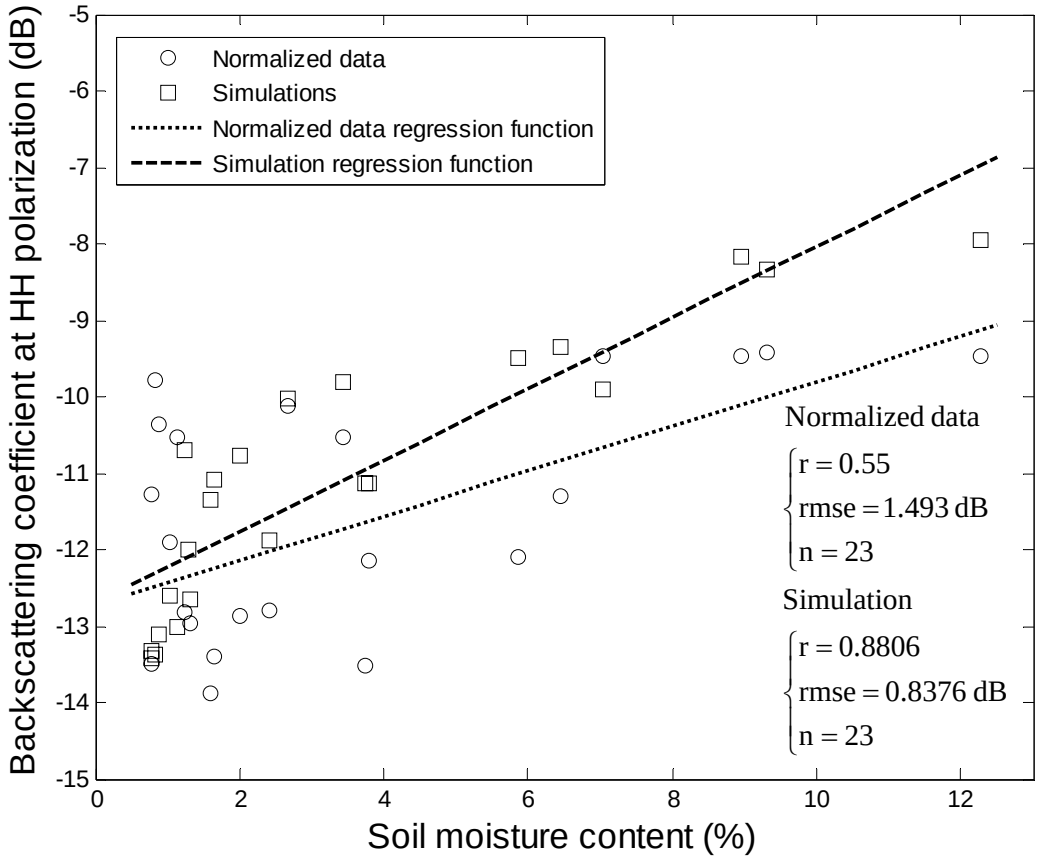
Normalized data
Simulations
Normalized data regression function
Simulation regression function
Normalized data
r = 0.55
rmse = 1.493 dB
n = 23
Simulation
r = 0.8806
rmse = 0.8376 dB
n = 23
Backscattering coefficient at HH polarization (dB)
Soil moisture content (%)
-5
-6
-7
-8
-9
-10
-11
-12
-13
-14
-15
0
2
4
6
8
10
12